SEMICONDUCTOR DIODE LASER DYNAMICS

APPENDIX 3

A

SEMICONDUCTOR DIODE LASER DYNAMICS

by

RANDALL EWEN PARK

PART A: ON-CAMPUS PROJECT

A project report submitted in partial fulfillment of
the requirements for the degree of
Master of Engineering.

Department of Engineering Physics
McMaster University
Hamilton, Ontario, Canada

1981

A

MASTER OF ENGINEERING (1981) McMASTER UNIVERSITY

Department of Engineering Physics Hamilton, Ontario

TITLE: SEMICONDUCTOR DIODE LASER DYNAMICS Part A

AUTHOR: Randall Ewen Park, B.Sc. (Simon Fraser University)

SUPERVISOR: Dr. B.K. Garside

Number of Pages: vii, 82

A

ABSTRACT

This report is a study of the dynamic properties of semiconductor laser diodes. The measurement of some important laser diode parameters necessary for dynamic behaviour prediction is described. The relaxation oscillation behaviour for laser diodes pumped with nanosecond time scale current pulses is predicted using both an approximate analytic solution and computer simulations. This predicted behaviour is compared with experimental results. Dynamic experiments with an external cavity for extra optical feedback and a regenerative loop for optoelectronic feedback are also described and discussed. Details of the experimental setups and techniques used are given.

ACKNOWLEDGEMENTS

The author would like to express his thanks to Dr. B.K. Garside for his supervision and encouragement. Thanks also to all the BSBSB guys and B.L.C. for their support. Special thanks to John Goodwin for numerous discussions and immeasurable help throughout this work.

TABLE OF CONTENTS

LIST OF ILLUSTRATIONS

1. INTRODUCTION

The semiconductor laser has emerged as an important component in optoelectronic systems. Its small size, relatively low cost, simple drive requirements, and fast response times have made it the source which makes long distance optical fiber communications viable. Diode lasers are also useful as fast pulse light sources for use in optical fiber testing, etc. For these applications, the diode dynamic response must be known and optimised.

The first demonstration of stimulated emission in GaAs diodes was in 1962[1-3]. Although there was much research in various compounds, early laser diodes operated only at cryogenic temperatures. The new process which made continuous room temperature operation possible in 1970 was the perfection of the heterojunction structure [4,5] (two adjoining single crystal semiconductors with dissimilar bandgap energies). Low defect heterojunctions were first realized using the lattice matching property of A1GaAs alloys, which enabled wide variation of the bandgap energy with negligible lattice parameter change.

A typical stripe contact, double heterostructure laser diode is shown in figure 1-1. (Additional heterojunctions are also commonly used to make control of the device parameters more precise, but the principal of operation is the same.) The active region is on the order of 1 μm thick, and has a higher index of refraction than the adjacent layers, producing a waveguide for optical confinement. The isotype heterojunction (n-n or p-p types) also forms a barrier for minority

FIGURE 1-1 DOUBLE HETEROSTRUCTURE LASER DIODE

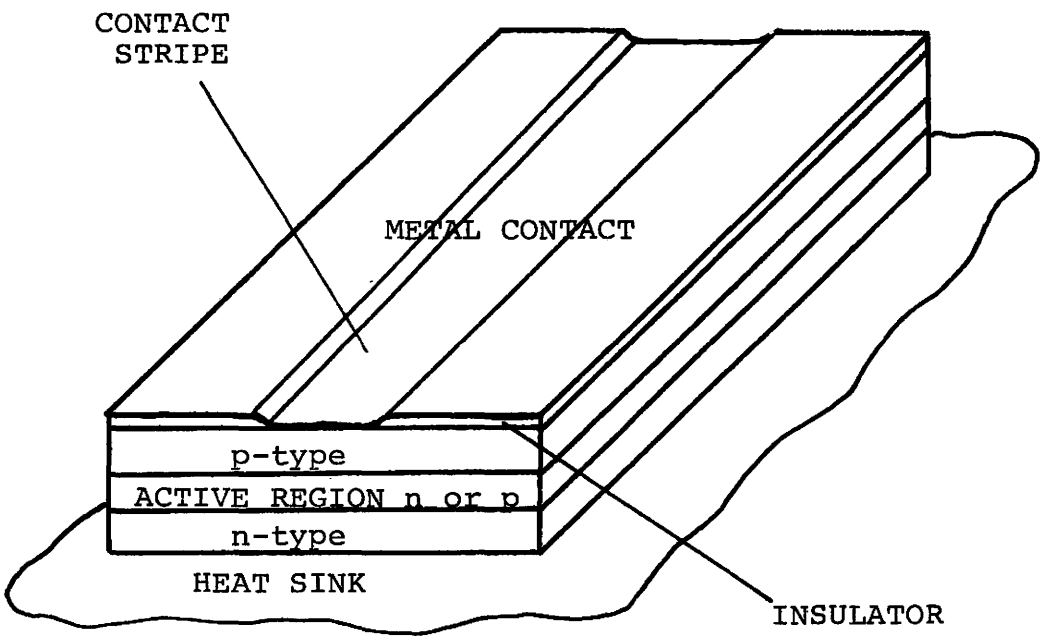

FIGURE 1-2 LASER DIODE SPECTRUM

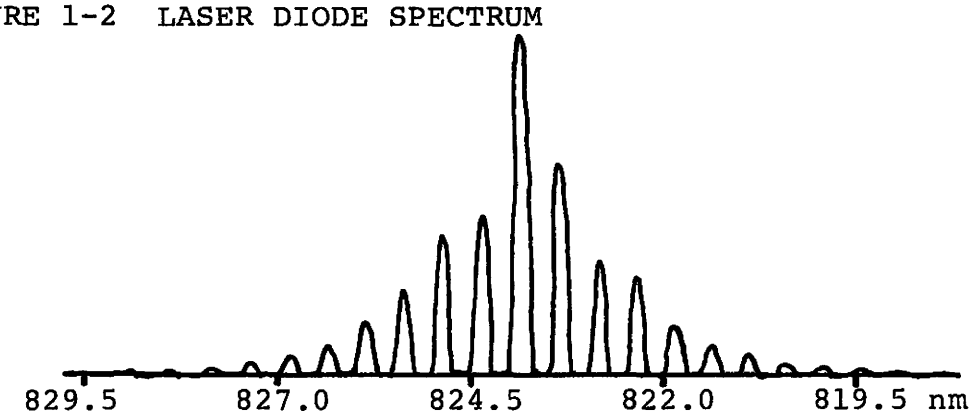

carrier confinement, and the anisotype heterojunction (n-p or p-n) improves the injection efficiency of the carriers. The stripe contact geometry serves to keep the carriers in a narrow region of the active area; this concentration of gain narrows the emitting aperture. The close confinement of photons and carriers is what enables low threshold currents, high efficiency, and room temperature operation.

The emitting area of the laser diode is typically 0.25 μm x 10 μm. The small emission area causes large diffraction effects, and the emission angles of a double or multi heterostructure laser diode are typically 70° by 10°. The emission wavelength for AℓGaAs lasers can be varied by varying the bandgap energy and a typical spectrum is shown in figure 1-2.

The one piece structure of laser diodes, where the mirrors are formed by the cleaved (and sometimes coated) ends, has the advantages of rugged construction, freedom from alignment problems, and compactness. However the same one piece structure means that it is not a simple matter to change the cavity length, the active medium length, or the mirror structure or reflectivity. The small dimensions of the laser diode layers and inhomogeneities associated with processing mean that local defects can have a large effect on the final laser behaviour. The high optical fields present inside the laser can also affect the laser characteristics, as in "hole burning", where the ideal homogeneous broadening situation is not followed.

A number of approaches have been used to model the behaviour of laser diodes. In order to use these models, parameters of the laser

diodes are needed.

To measure the laser diode parameters it is necessary to infer information about what is happening inside the laser diode by its response to outside effects. In this work, various techniques were used to measure the major parameters controlling laser dynamics.

Chapter 2 describes the basic experimental apparatus and techniques used with the laser diodes. The high speed pulse generating circuits used to drive the lasers, as well as the microwave response laser diode mounts are described. The optical and electronic feedback systems used are outlined.

Chapter 3 describes the measurement of two important laser diode parameters, the threshold current and the carrier spontaneous recombination time. The threshold current was measured both c.w. and pulsed, and the difference between the two values is discussed. The carrier spontaneous lifetime was measured using the time delay between the application of a pumping pulse and light emission.

Chapter 4 discusses theoretical predictions and experimental results of the laser diode dynamic response to fast current pulses on a picosecond time scale. Small signal and computer simulation techniques are used to predict the dynamic behaviour, and comparison is made with experimental results. Explanations are proposed for other effects which affect the accuracy of the predictions.

Chapter 5 describes theoretical and experimental results for the laser diode operated with an external mirror to produce extra optical feedback. The c.w. and dynamic effects of the external cavity are

described and compared to computer simulations.

Chapter 6 describes a laser diode system with an optoelectronic feedback loop, producing a regenerative pulser system. Performance of the pulser is given as a function of loop parameters.

Chapter 7 gives conclusions.

2. EXPERIMENTAL APPARATUS AND TECHNIQUES

2.1 Diode Laser Drive Methods

The laser diodes used in these experiments were all room temperature c.w. multiheterostructure type, with c.w. threshold currents (I_{th}) of 130 to 190 mA. The lasers were operated in both c.w. and pulsed mode. Current pulses for the laser diodes were produced using avalanche transistor pulsers because of their simple construction, fast risetime current pulses, and high repetion rates.

The principle of operation of an avalanche pulser is illustrated in fig 2-1. The capacitor C, which may be a discrete component or a form of transmission line, is charged through resistor R to the voltage V_{cc}. The R-C relationship governs the maximum repetition rate for complete capacitor charging. To produce the voltage pulse, the transistor is triggered by a positive current pulse into the base, causing the transistor to avalanche and the capacitor to discharge through R_L (typically 50Ω). The voltage V_{cc} must be large enough to cause the transistor to avalanche, but less than the voltage at which the transistor avalanches spontaneously. The 2N708 was the transistor used in all the experiments here because it had the fastest risetime and was able to produce current pulses up to approximately 2 I_{th}.

Microstrip circuits made using double sided epoxy glass printed circuit board were used for most of the pulsers because of their ease of construction. A microstrip transmission line consists of a strip of copper separated form a ground plane by a dielectric (fig 2-2). Lumped

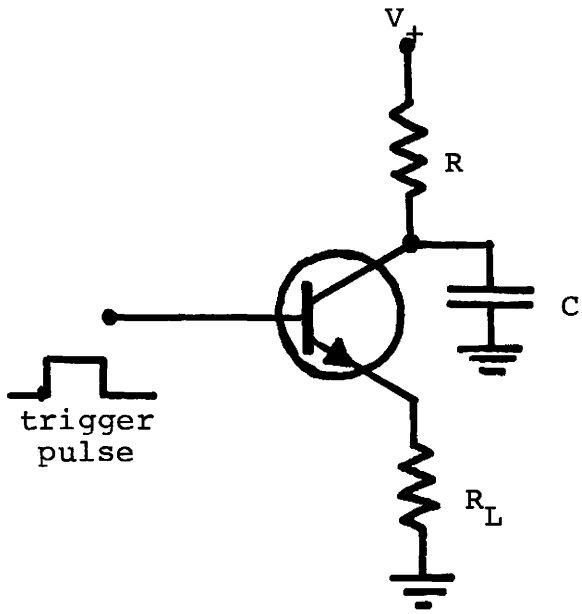

FIGURE 2-1 AVALANCHE TRANSISTOR PULSER

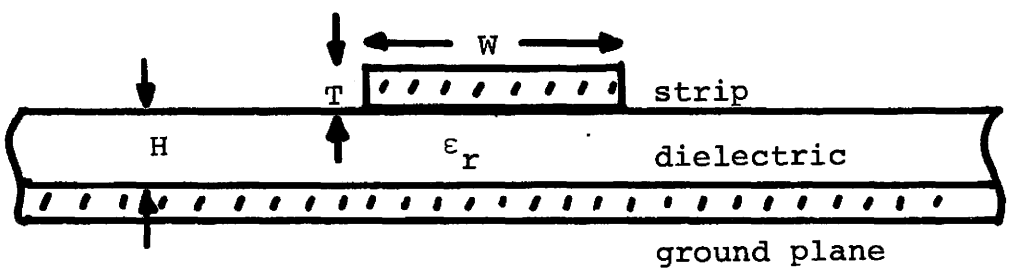

FIGURE 2-2 MICROSTRIP TRANSMISSION LINE

components can be simply soldered to the stripline if the frequency of operation is not too high for the components themselves. Microstrip to coaxial adaptors can be mounted through the board (fig 2-3) or end launched (fig 2-4) with losses typically 1dB at 10 GHz[6]. The main disadvantage of epoxy glass as a dielectric is its high loss (typically 5 dB/m at 5 GHz), but for the short distances used here, this was not a problem.

Various values for the dielectric constant of epoxy glass were obtained from different sources, ranging from $\varepsilon_r = 3.6$ to $\varepsilon_r = 5.2$. An experimental measurement of the capacitance of a sheet of double sided epoxy-glass board gave a value of ε_r which extrapolated[7] to 4.4 at 1GHz.

Numerous formulae exist for estimating the stripline impedance (i.e. 6-8); one which takes the most effects into account is given by John and Arlett[8]:

$$Z_o = \frac{\xi}{\sqrt{\varepsilon}} \left[\frac{W}{H} + \frac{C_2 W}{H\sqrt{\varepsilon}} + \frac{C_1}{\log(4H/T)}\right]^{-1} \qquad 2\text{-}1$$

where $\varepsilon = 0.4475\ \varepsilon_r + 0.6965$

$C_1 = 0.0515\ (H/T) + 2.183$

$C_2 = -0.6895\ \{H/(\varepsilon W)\} + 1.2163$

ξ = free space impedance

and W, H and T are as in fig. 2-2

The strip width for 50Ω impedance microstrip using 1 oz. copper board with 0.0625" dielectric ($\varepsilon_r = 4.4$) was calculated using this formula and was almost exactly 0.1". Tests were made on a 0.1" stripline using a Hewlett Packard time domain reflectometer (TDR) and the board impedance

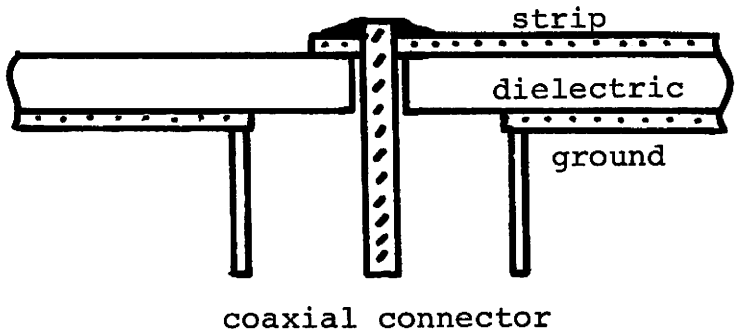

FIGURE 2-3 90° MICROSTRIP LAUNCHING

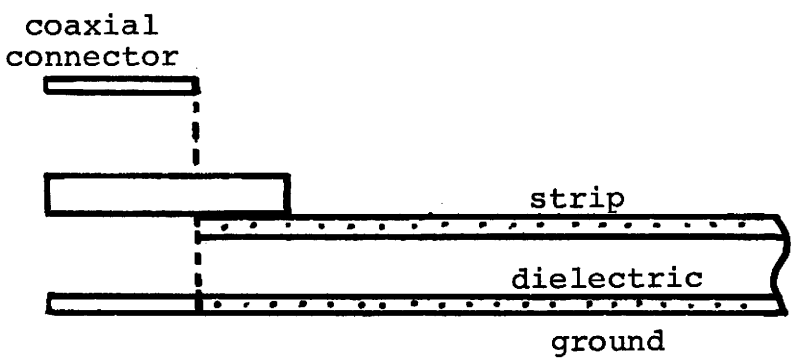

FIGURE 2-4 END MICROSTRIP LAUNCHING

was 50 $\pm$ 1Ω. These tests also showed that end launched SMA connectors had the lowest reflection coefficient for coax-stripline transitions (reflection coefficient ρ = 0.03) and that reflections from inline chip capacitors were also very low (ρ = 0.03 for two capacitors mounted side by side, each half the strip width wide).

Various stripline type avalanche pulsers were constructed as the requirements were modified (to allow for a d.c. laser bias for example) and the circuits were investigated. It was found that a coaxial cable as a discharge line gave better pulse risetime and shape than a stripline discharge line. A single section L-C filter was used to isolate the pulser from a low voltage power supply used for d.c. laser bias. Inline chip capacitors were used for the capacitance (fig 2-5) which was necessary to prevent the avalanche circuit from being affected by the laser bias. The inductor used was typically 20 turns of wire on a 1K, 1/4 W resistor. It was found that the best arrangement for the laser bias section was to have it on a separate board from the avalanche transistor. This enabled attenuators to be inserted between the avalanche board and the bias board, since the avalanche pulses only have fast risetimes and flat tops over a limited output range. With this configuration, the d.c. doesn't go through the attenuators and there is no problem with power dissipation in the attenuators.

The analysis and experiments above enabled reduction of the pulser risetime from the original 400 psec to 300 psec, and gave a pulse with less pulse droop. Subsequent to this work when a new pulser was being built to replace an old one, thought was given to the optimum

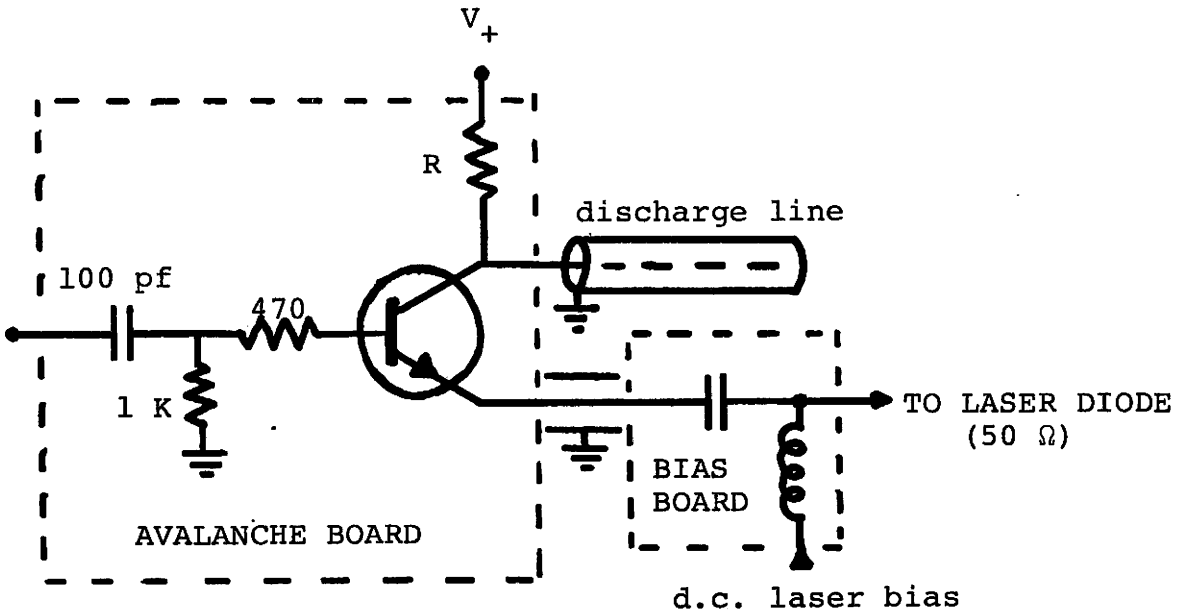

FIGURE 2-5 PRACTICAL AVALANCHE PULSER

length of stripline between the transistor leads and the SMA connectors. It was decided to try eliminating the stripline altogether. Thus a new pulser (fig 2-6) was constructed, with the transistor leads mounted directly to two end to end SMA connectors in a semi-coaxial mount. The pulse output (fig 2-7) had less droop than the previous designs and a much faster risetime (200 psec).

A pulser was also tried with the 2N708 chip removed from its case and mounted directly on a stripline circuit. This did not give any improvement in risetime however, and the pulse top was not as flat as with the previous pulser.

2.2 Diode Laser Mounts

Due to the different packages of the lasers used, various laser mounts were constructed. The three laser packages used are shown in figs 2-8 a), b), and c). To interface the lasers with the pulsers, it was necessary to have the lasers act as 50Ω terminations. The lasers also had to be optically accessible. For laser #1, a coaxial package using an N-type connector was made (fig 2-9). The stud was the positive terminal on this laser, and went to the center conductor for positive pulse inputs while the lead was connected to ground through a 50Ω, 2 W resistor. While this mount was never tested on the TDR, it seemed to work well.

Laser #2 was the easiest to mount well. A GR 874 series component mount (fig 2-10) was used as the basis of this mount. New sections of center conductor were made, and the laser was soldered in

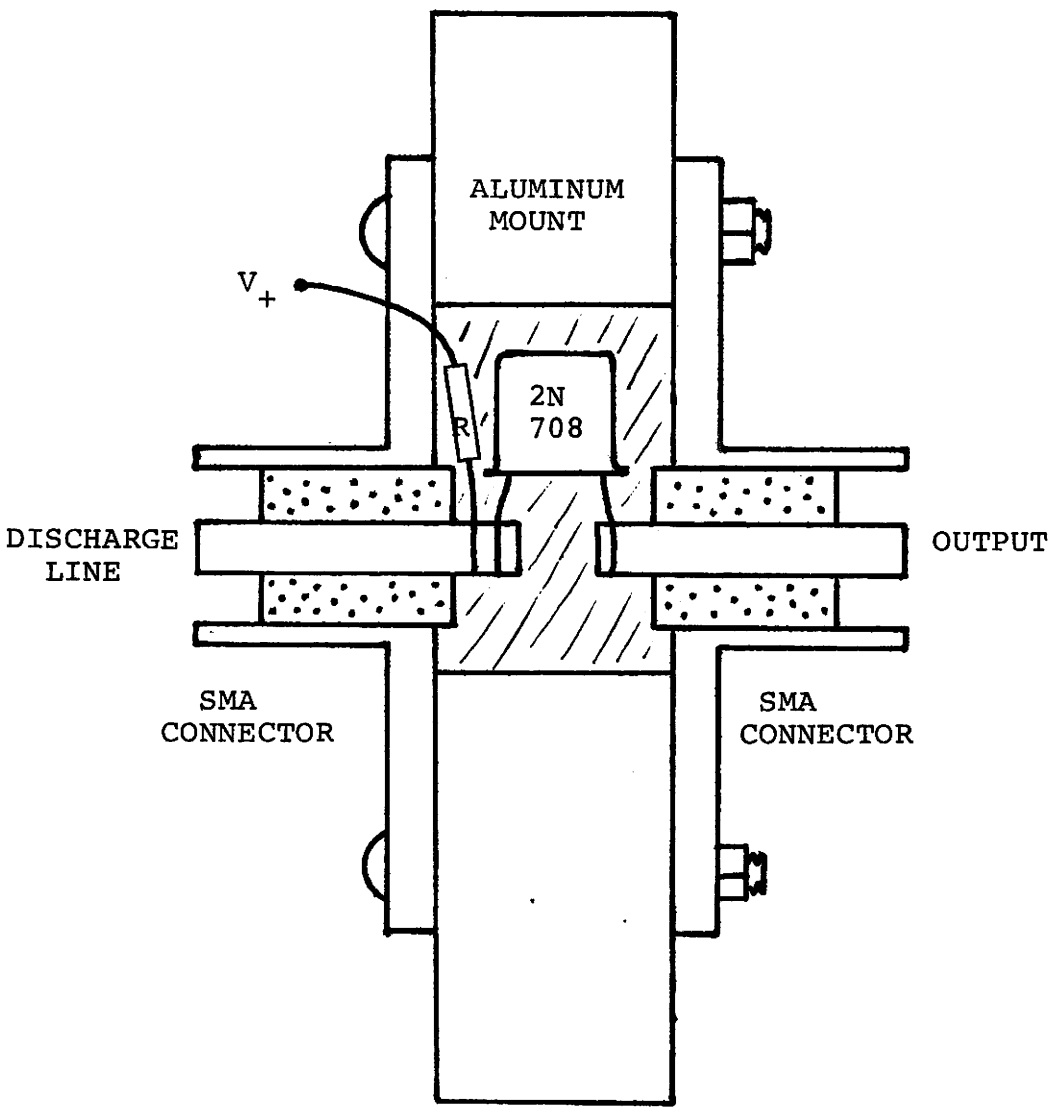

FIGURE 2-6 COAXIAL AVALANCHE PULSER

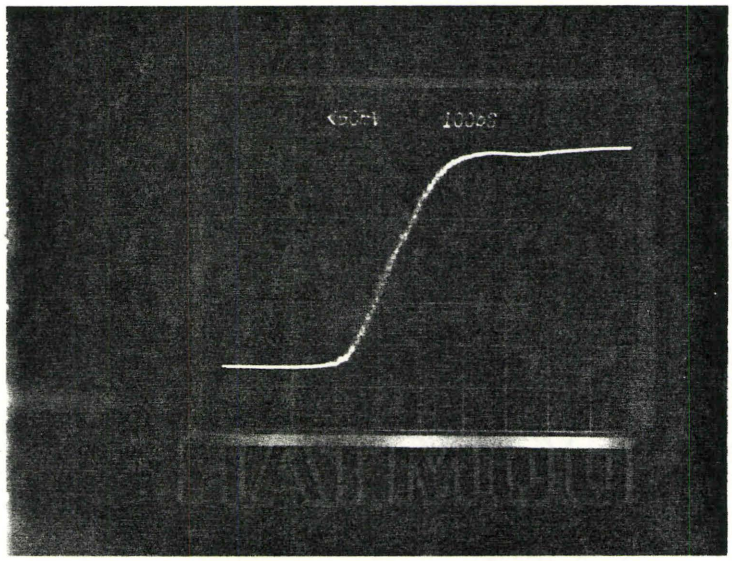

100 psec/cm

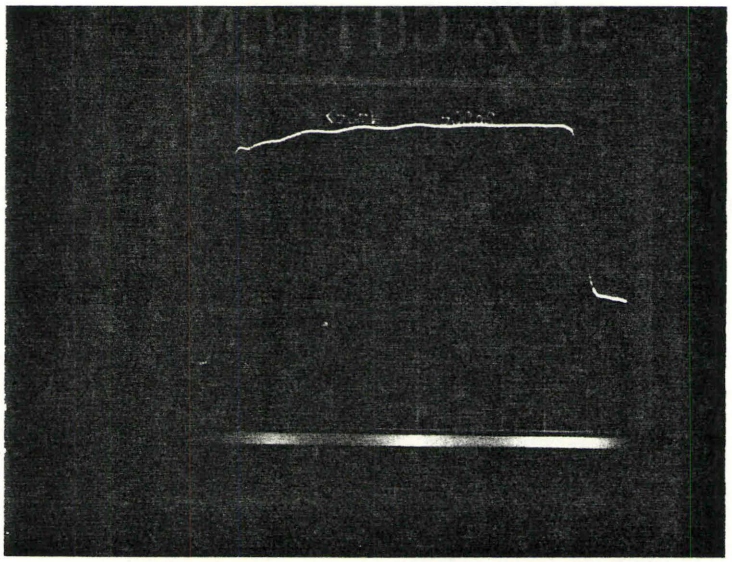

500 psec/cm

FIGURE 2-7 COAXIAL PULSER OUTPUT

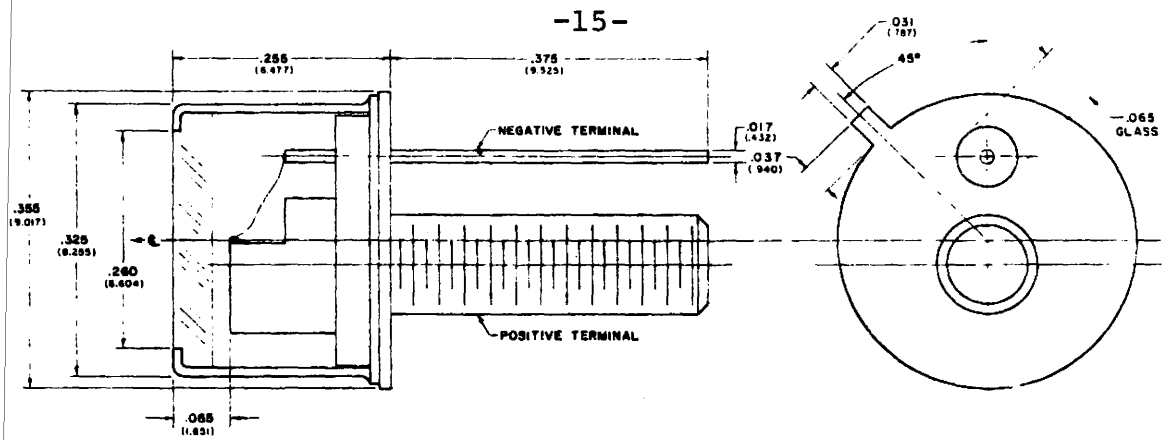

(a) laser #1

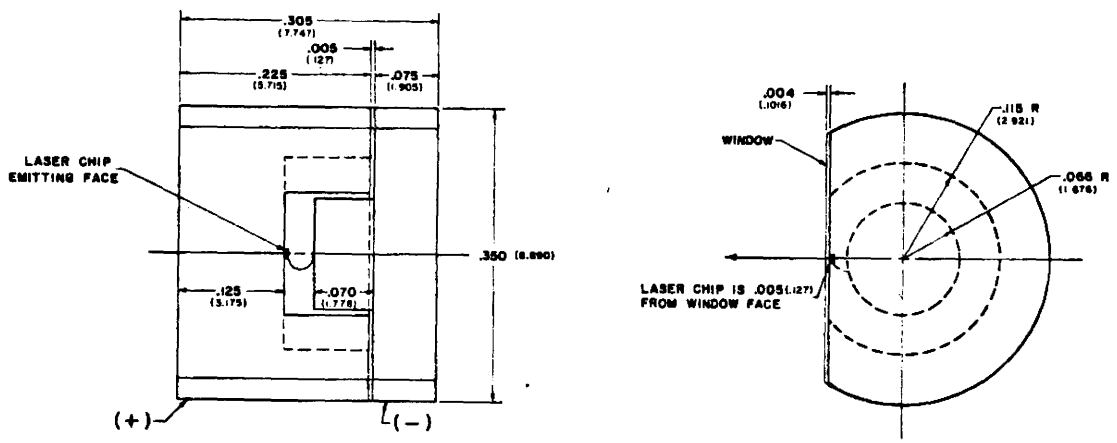

(b) laser #2

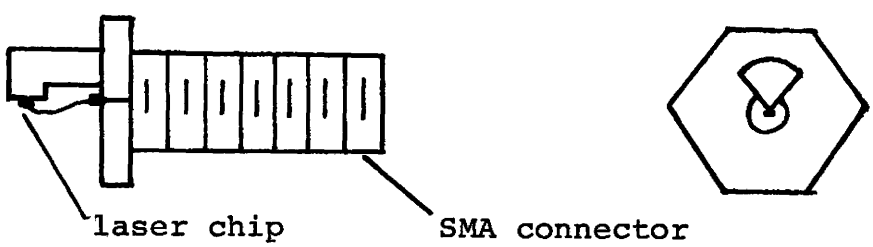

(c) laser #3

FIGURE 2-8 LASER DIODE PACKAGES

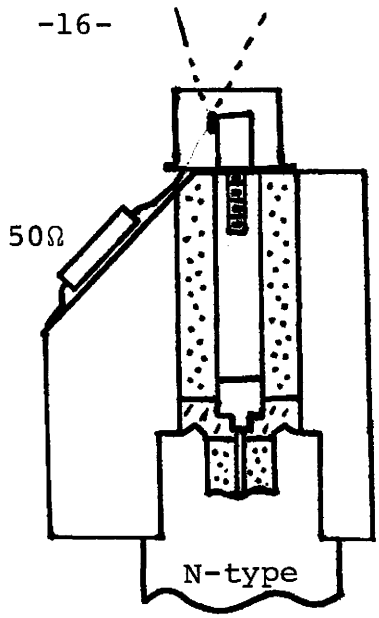

FIGURE 2-9 LASER #1 MOUNT

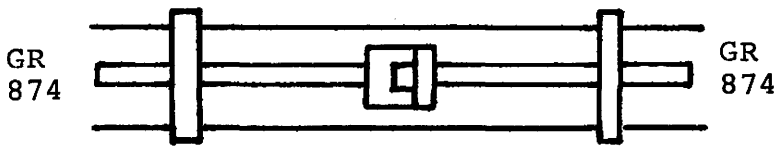

FIGURE 2-10 LASER #2 MOUNT

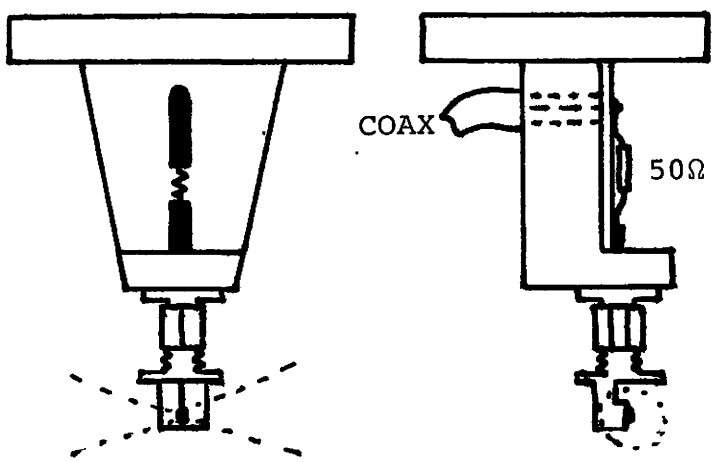

FIGURE 2-11 LASER #3 MOUNT

series with the 6mm diameter center conductor. A new outer conductor with a hole for optical access was made out of 13 mm i.d. tubing. In this way the change in diameter from the center conductor to the laser introduced reflections of less than 10%. In addition, the 50Ω impedance can be obtained by terminating either end of the mount with 50Ω (this can be a 50Ω attenuator to monitor the actual laser current), allowing the laser to be used with either positive or negative pulsers. TDR tests gave a reflection coefficient < 0.1.

For laser #3, a negative mount was used (fig 2-11) because the center conductor of the SMA connector went to the negative laser terminal. A mount was machined and a 50Ω series resistor was used to match to the pulser. For d.c. laser bias, a coil was mounted in series with the d.c. supply and an external coupling capacitor was used with the pulse source.

2.3 Optical Detectors

Three different optical detectors were used in these experiments. The one used for most of the early experiments was an Opto-Electronics Ltd. PD-10 silicon photodetector with a full width half maximum (FWHM) of 210 psec for a δ-function input. The second detector used was a prototype from Opto-Electronics Ltd. with a FWHM of 150 psec. The third detector was again an Opto-Electronics Ltd. prototype, this one having a FWHM of 60-70 psec.

2.4 Measuring Dynamic Responses

For observation of relaxation oscillations, a simple source-lens-detector arrangement was used (fig 2-12). The lenses used were 25 to 30 mm diameter and approximately f 1 to 2. Since the photodetector active areas were 0.5 mm by 0.5 mm, there was no problem with aberrations using just simple lenses.

2.5 External Cavity Optics

The optics for the external resonator experiments were deceptively simple. The simplest form of the resonator consisted of an external lens to collimate the laser light and a plane mirror to provide the optical feedback (fig 2-13). However the choice of the lens and mirror, as well as their alignment, was crucial to the operation of the cavity. Lasers #1 and 2 had only one facet accessible, and thus to see the optical signal it was necessary to tap part of the feedback signal. The first arrangement used was a partially reflecting mirror (fig 2-14). The mirror used had 40% transmission at 0.8 μm, and although it was tried with various lenses at various times, it did not provide enough optical feedback for a really good effect.

The final arrangement used for the mirror section is shown in fig 2-15. Here a silicon flat was used (99% reflectivity) for feedback, and the optical signal was tapped off using a microscope slide as a beam splitter. Although the detected signal was small (signal averaging had to be used in most cases), this arrangement permitted approximately 88% of the light to be returned, and in addition provided a means of looking

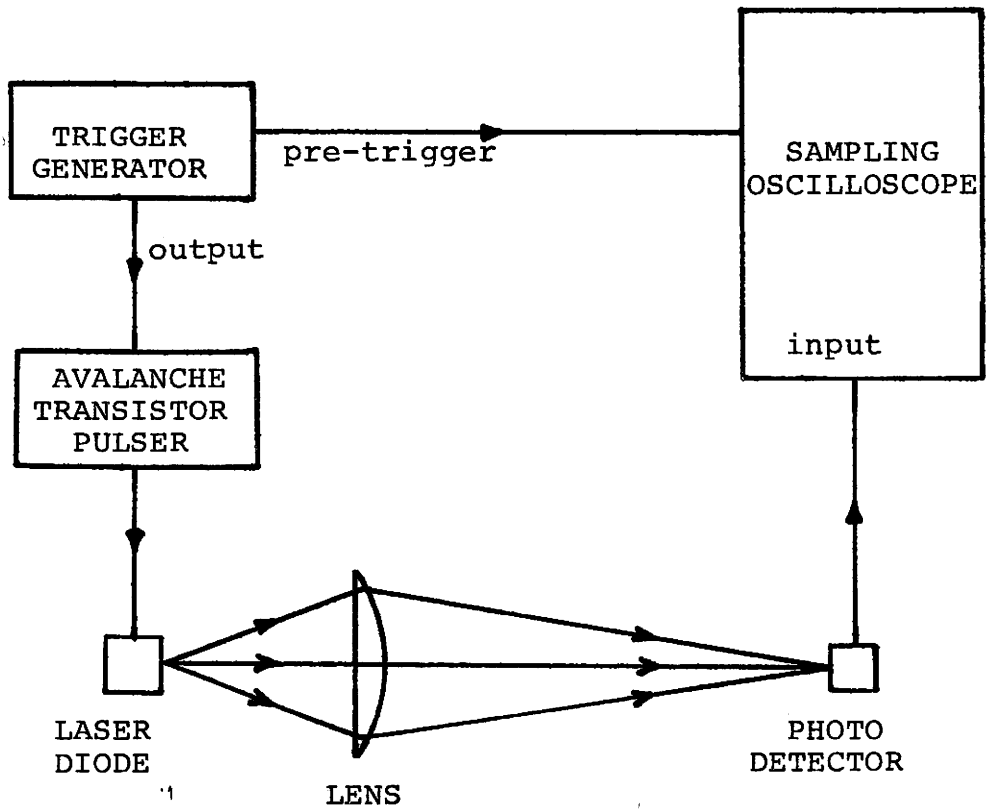

FIGURE 2-12 DYNAMIC OBSERVATION SETUP

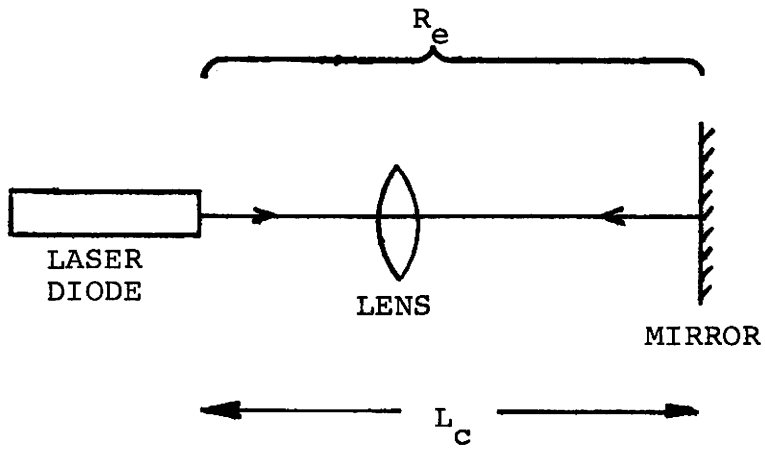

FIGURE 2-13 EXTERNAL CAVITY

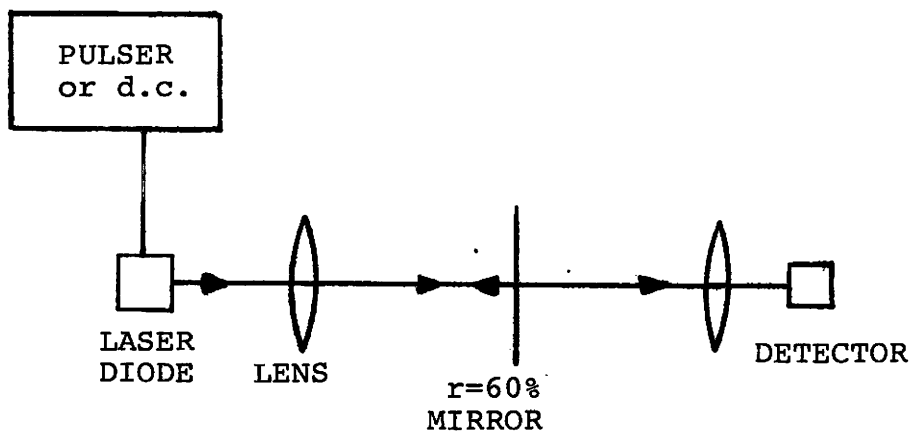

FIGURE 2-14 EXPERIMENTAL EXTERNAL CAVITY #1

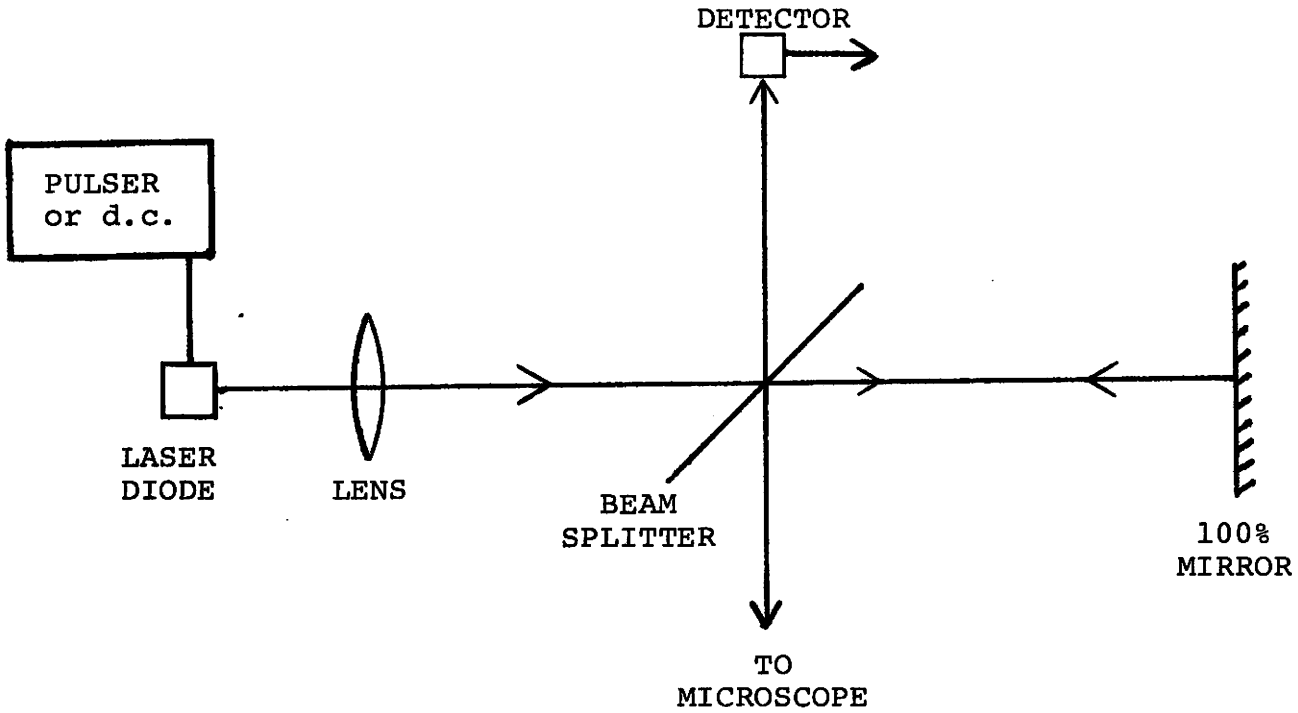

FIGURE 2-15 EXPERIMENTAL EXTERNAL CAVITY #2

along the cavity axis with a microscope (discussed in section 2.6).

It was realized after many trials with different lenses that to get good effects from the external cavity a microscope objective had to be used to collimate the laser light. One inch diameter plano convex lenses were first used in various compound combinations, but the aberrations prevented the formation of a sharp image back into the laser active region. The problem with microscope objectives was their short working distances (from the front face of the objective to the object). Since the numerical aperture of the objective increases with increasing magnification, it was desirable to have a high power objective, but the working distance decreases with increasing magnification which caused problems with some of the laser mounts. Laser #2 for example was mounted with the laser chip pointed down into the mount at an angle of approximately 9^{o}. Thus the microscope objective could not be brought very close to the laser, because the edge of the objective hit the laser mount (fig 2-16). With laser #1 (after the cap was removed) it was possible to use a 20X, 0.5 N.A. objective; with lasers #2 and 3 only 10X, 0.25 N.A. objectives could be used.

2.6 External Cavity Alignment

Accurate alignment of the external resonator system was essential in order to see cavity effects. The mirror tilt was obviously the most sensitive adjustment, and standard commercial 1 arc second resolution mirror mounts were found to be too coarse. Thus a new mirror mount with 15 cm lever arms for the micrometers was machined. It pivoted on one

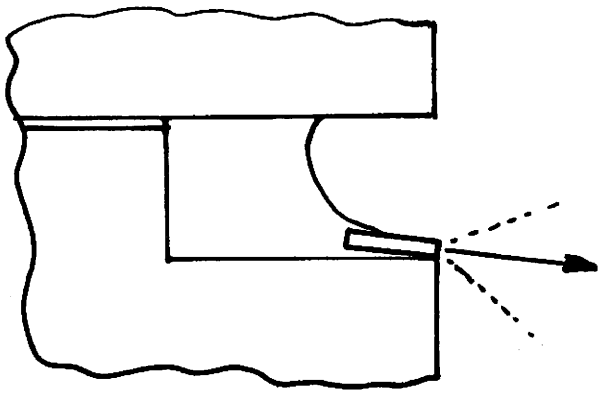

FIGURE 2-16 LASER #2 CHIP ORIENTATION

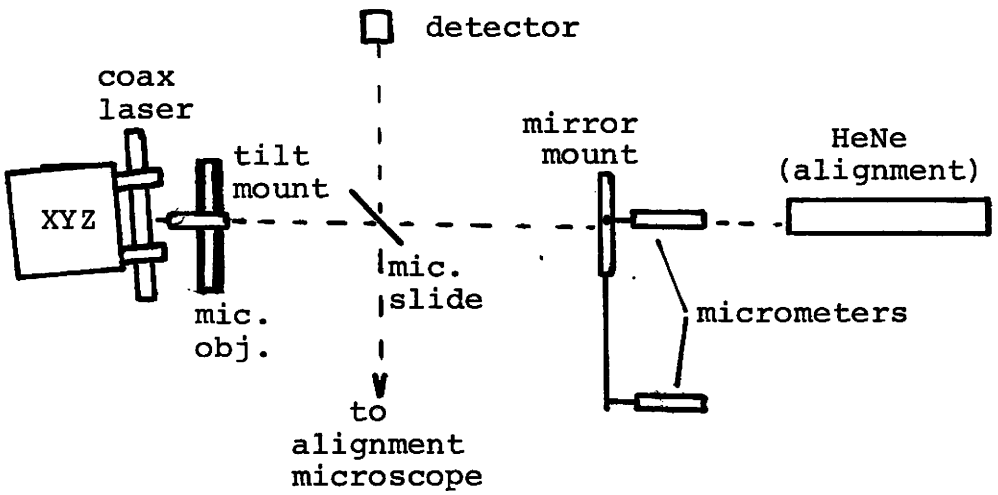

FIGURE 2-17 EXTERNAL CAVITY SETUP

ball bearing and the two micrometer ends and had a resolution of better than 0.25 arc seconds. Due to problems with vibrations, all the optical components were clamped right to the table, with the optical axis being approximately 30 mm above the table surface. The microscope objective was mounted in a standard mirror mount to give angular adjustment and the laser diode was mounted on an X-Y-Z positioner to give linear adjustments (fig 2-17).

The procedure used to align this cavity (and similar setups) used a HeNe laser and was as follows:

1. The HeNe beam was set at the appropriate height (≈30mm), approximately parallel to the table. This HeNe beam defined the optical axis for the system. The spot where the HeNe beam struck the wall behind the setup was also marked.
2. The laser diode on the X-Y-Z positioner was inserted in the HeNe beam and the diode axis was aligned parallel to the HeNe by adjusting the angles of the laser diode so that the reflection from its face exactly entered the HeNe. The reflection was easily identified as the diffraction pattern from a rectangular slit, with the central maximum approximately 2 mm by 5 mm at a distance of 1 m. With the HeNe 1 m away, these angles can be accurate to $\pm$ 2' of arc.
3. The laser diode was then translated in one direction so that it was out of the optical path. The lens or objective was then inserted and the lens position (2 axes) and angle (2 axes) were adjusted by observing both the transmitted and reflected beams of the HeNe. The reflected beam was centered on the HeNe face and the transmitted beam

was centered on the marked spot on the wall.

4. The laser diode was then translated back into the beam. When the laser chip was in position, a bright reflection could be seen back on the HeNe. Final adjustment was made by turning the laser diode on and centering its beam on the HeNe.
5. The laser diode was moved along the optical axis to get a parallel beam from the objective. The mirror was then inserted and roughly aligned.
6. The microscope, with the infrared viewer at one eyepiece, was then used to view the operating (c.w.) laser using the beam splitter. As the cavity mirror was adjusted, the reflected image was visible on the laser chip. The final step was to bring the two images into coincidence, using the mirror adjustments and the focussing micrometer on the laser X-Y-Z.

2.7 Optoelectronic Regenerative Pulser

The experimental arrangement for the optoelectronic feedback system is shown in figure 2-18. Laser diode #3, with access to both facets, was used in this system. The optoelectronic feedback loop consisted of a 210 psec FWHM detector, a pulse amplifier chain, and a pulse sharpener which drove the laser diode. The amplifier gain was 57 dB and pulse risetime was 1 nsec. The pulse sharpener board contained a series capacitor high pass filter, a current pulse tap, and a standard two step recovery diode (SRD) pulse shaping circuit (fig 2-19). A step recovery diode is normally forward biased by a constant current source,

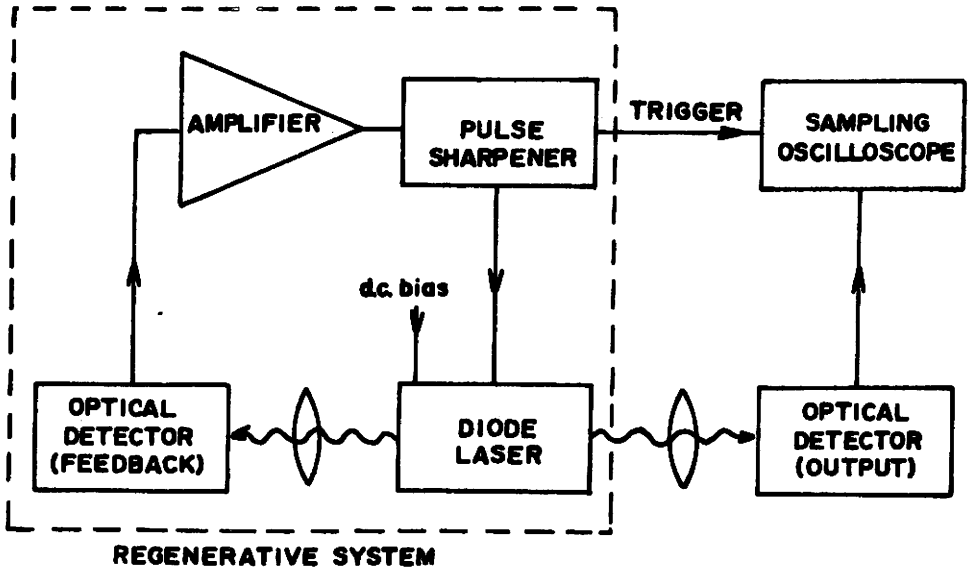

FIGURE 2-18 OPTOELECTRONIC FEEDBACK SYSTEM

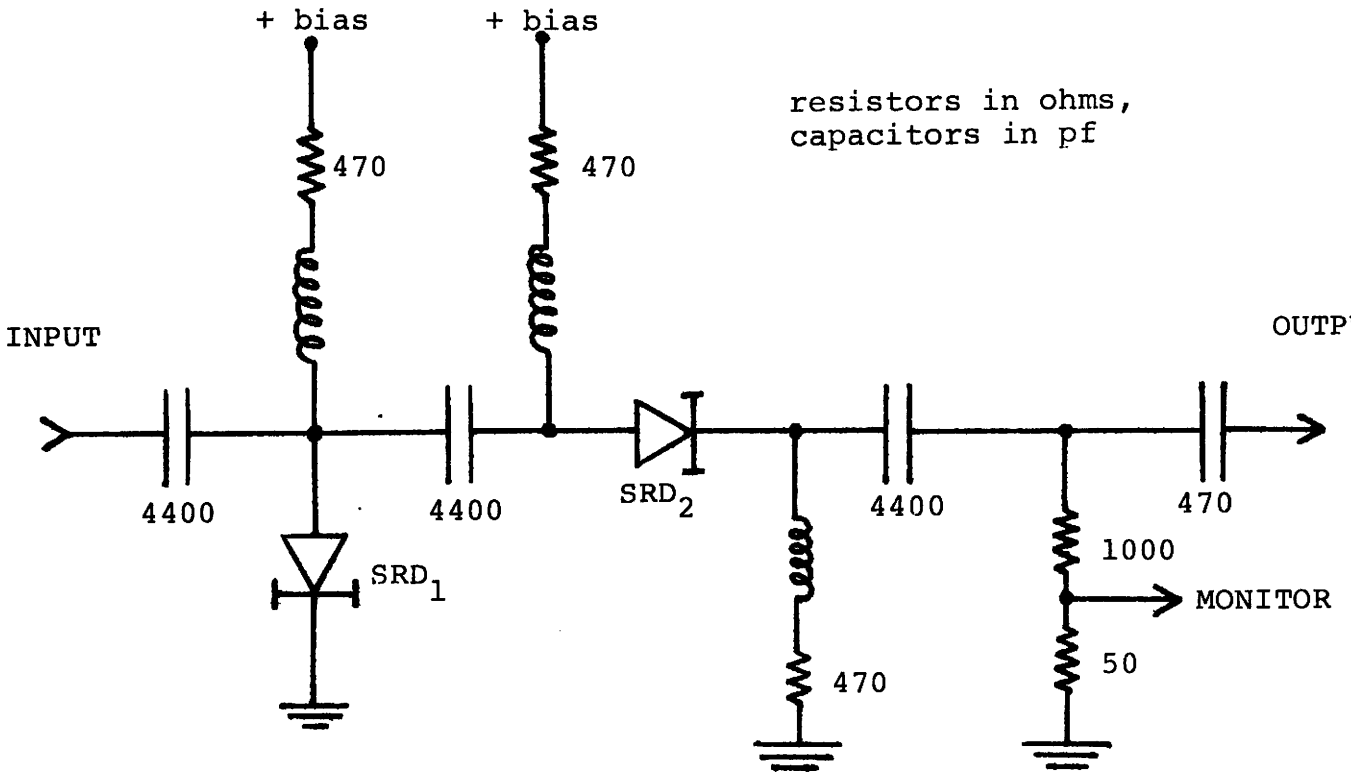

FIGURE 2-19 STEP RECOVERY DIODE PULSE SHAPER

and connected such that the current pulse to be shaped reverse biases the diode. Thus in fig 2-19, SRD_1 appears as a short to ground until the input pulse depletes the stored charge. The diode then switches rapidly to reverse biased and an open circuit, and the pulse risetime is now approximately the SRD switching time. This switching time can be as short as 50 psec[10].

SRD_2 in this circuit again appears as a short until its charge is depleted, and it switches, cutting off the back end of the pulse and producing a fast fall time. Thus the pulse length can be adjusted by varying the bias current and thus the charge stored by SRD_2.

3. DIODE LASER PARAMETER MEASUREMENT TEQUNIQUES

3.1 c.w. Threshold Current

The most important parameter of a diode laser is its threshold current (I_{th}). Since 1970, room temperature c.w. operation of diode lasers has been possible because of reduced threshold currents. The room temperature c.w. diode lasers use double or multi heterostructure construction and stripe geometry which provide close confinement of both optical and electrical energy, making low (<200 mA) threshold operation possible. The total power dissipation of the laser diode is the limiting factor here, since the diodes are very small (typically 200 μm x 200 μm x 50 μm).

The threshold current in diode lasers is strongly temperature dependant. The dominant effect is the need for more carriers in the recombination region to maintain a given gain coefficient with increasing temperature. Other effects are decreases in carrier and radiation confinement with increasing temperature. The approximate dependance is $I_{th} \propto T^b$, where $b \simeq 1.5$ at room temperature[11]. Thus even a change in diode temperature of 5^oK can change the threshold by 3%.

This change of I_{th} with temperature is the primary reason for the difference between the I_{th} for a nsec type pulse and the I_{th} for d.c. operation. For low duty cycle, fast pulses the laser does not have time to heat up and the I_{th} is effectively lower than that for the d.c. case. In the latter, when the laser is in thermal equilibrium with its surroundings, it will be a few degress (depending on the mount) hotter

FIGURE 3-1 LIGHT vs. CURRENT CHARACTARISTICS

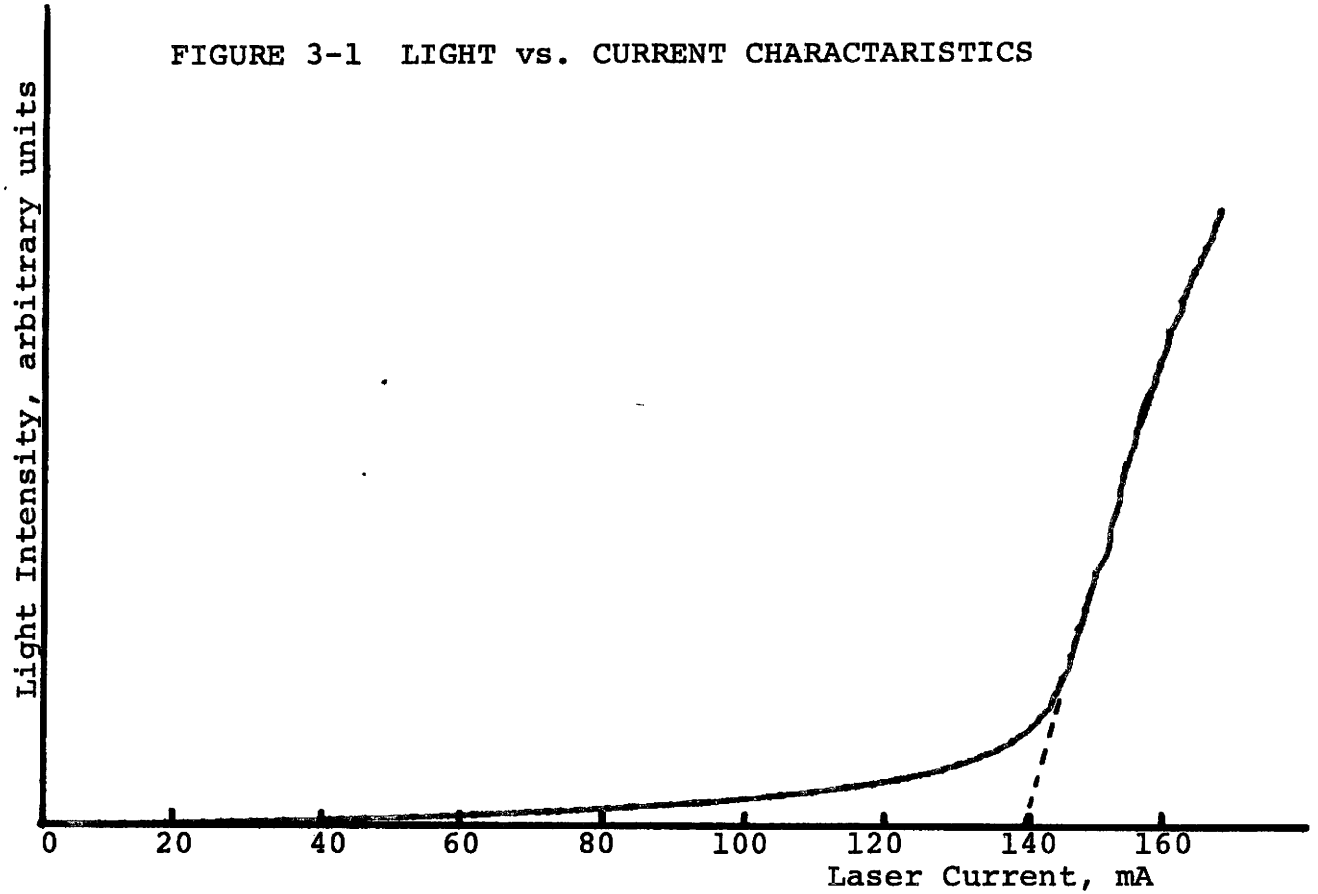

than room temperature, increasing the I_{th}.

Measurements of the d.c. I_{th} are usually done by taking a light intensity vs. current (L-i) curve. Threshold current is defined as the point where an extension of the lasing slope of the curve crosses the axis (fig 3-1).

Experimentally the L-i curves were obtained by increasing the current linearly from 0 to 1.2 I_{th} over a period of approximately 30 seconds. The current was increased and decreased in this manner once before each curve was taken to ensure that the laser cycled through the same temperatures for each run. This resulted in reproducibility of better than $\pm$ 0.3% on any part of the curve.

3.2 Spontaneous Carrier Recombination Time τ

Consider a recombination region d wide. The injected carrier pair density ΔN within this region as a function of time is[11]

$$\frac{\partial(\Delta N)}{\partial t} = J/ed - \Delta N/\tau \qquad 3\text{-}1$$

where τ is the spontaneous carrier recombination time, J is the injected current density, and e is the electron charge. If the dependance of τ on ΔN is neglected, this expression can be integrated to get the time delay between application of a step function drive current and the onset of lasing when $\Delta N = (\Delta N)_{th}$:

$$t_d = \int_{\Delta N_{d.c.}}^{\Delta N_{th}} \frac{d(\Delta N)}{(J/ed - (\Delta N)/\tau)}$$

$$t_d = -\tau \ln \left[\frac{J}{ed} - \frac{\Delta N}{\tau}\right]_{\Delta N_{dc}}^{\Delta N_{th}} \qquad 3\text{-}2$$

In steady state, $\frac{\partial(\Delta N)}{\partial t} = 0$ and equation 3-1 gives

$$(\Delta N)_{th} = \frac{J_{th}\,\tau}{ed} \qquad 3\text{-}3$$

and

$$(\Delta N)_{d.c.} = \frac{J_{dc}\,\tau}{ed} \qquad 3\text{-}4$$

Substituting 3-3 and 3-4 into 3-2 gives

$$t_d = \tau \ln \left[\frac{J/_{ed} - J_{dc/ed}}{J/_{ed} - J_{th/ed}}\right]$$

or in terms of current

$$t_d = \tau \ln \left[\frac{I_{pk} - I_{dc}}{I_{pk} - I_{th}}\right]$$

$$t_d = \tau \ln \left[\frac{I_{pulse}}{I_{pk} - I_{th}}\right] \qquad 3\text{-}5$$

where I_{pulse} is the current pulse amplitude, and I_{pk} is the total (d.c. + pulse) current amplitude. Measurements of the delay t_d as a function of applied currents were done on laser diode #2 and are plotted in figures 3-2 and 3-3. Figure 3-2 shows t_d as a function of $\ln(I_{pulse}/(I_{pk} - I_{thp}))$ (equation 3-5) where I_{thp} is the pulsed threshold current. The slope of this line equals the carrier lifetime

FIGURE 3-2 LASING DELAY vs. LASER CURRENTS

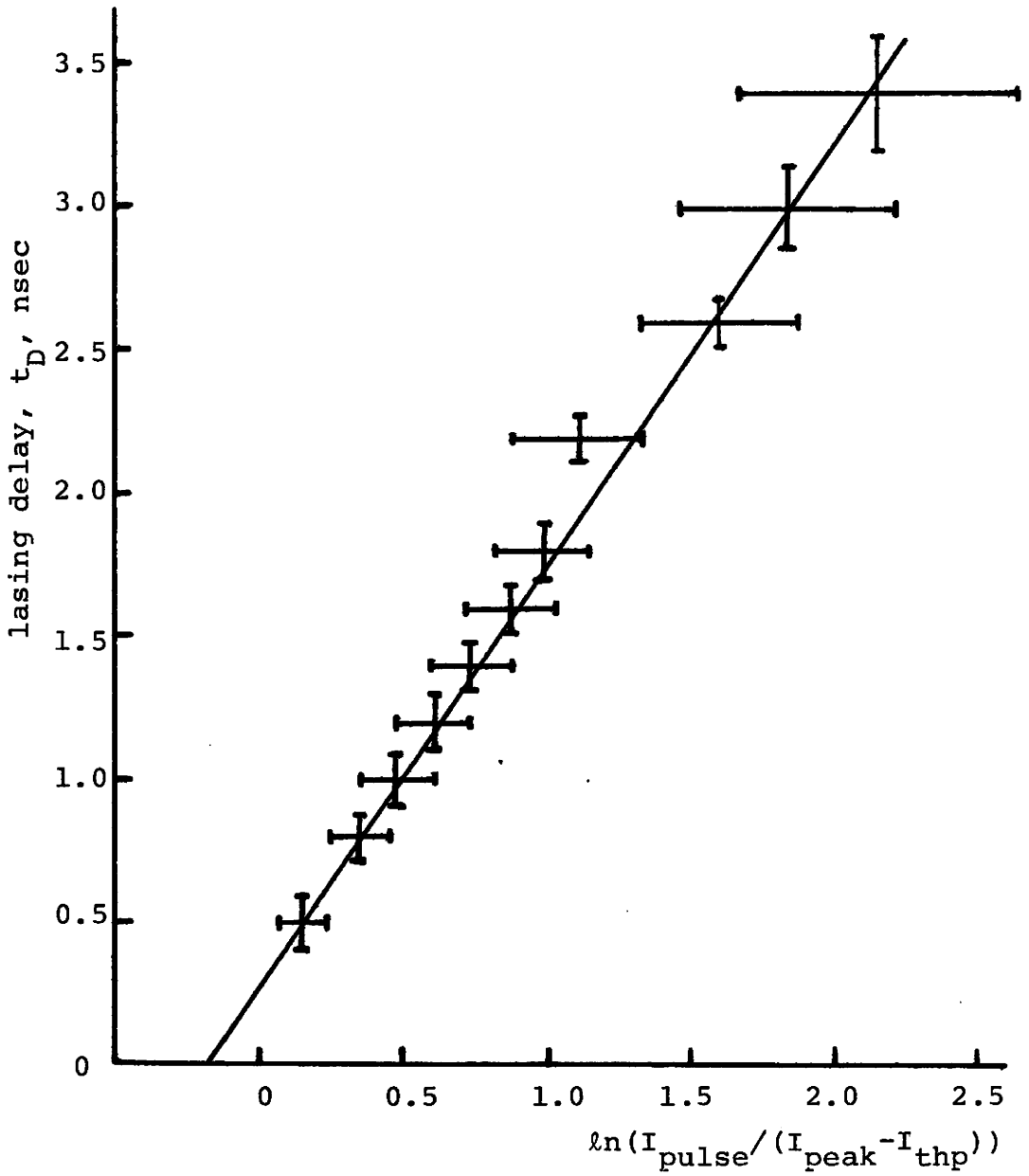

FIGURE 3-3 PEAK CURRENT vs. TIME DELAY, CARRIER LIFETIME

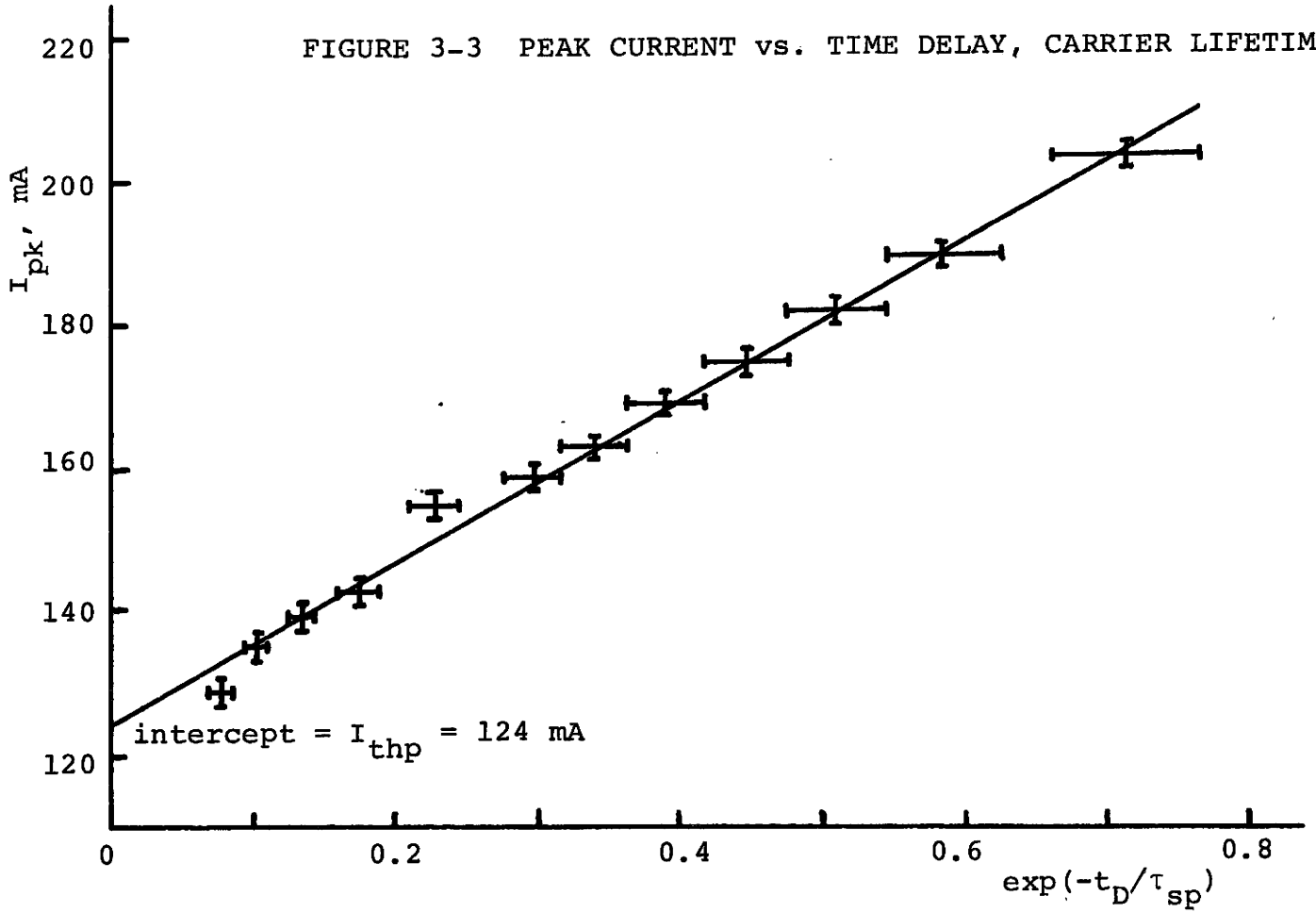

τ, and was τ = 1.5 $\pm$ 0.2 nsec, in agreement with other workers[11]. The value of I_{thp} was obtained by decreasing the current pulse amplitude until no light could be measured (-25dB).

To check the value for I_{thp}, the same data with the new value for τ was plotted as (figure 3-3)

$$I_{peak} = I_{thp} + \frac{I_{pulse}}{\exp(- t_d/\tau)} \qquad 3\text{-}6$$

This confirmed the value of I_{thp} as 124 $\pm$ 3 mA, 11% below the c.w. threshold current.

4 LASER DIODE RELAXATION OSCILLATIONS

4.1 Rate Equations

The dynamic behaviour of laser diodes can be modelled using two coupled equations for the electron and photon densities. The simplifying assumptions used here are:

1) All parameters are uniform inside the laser cavity, 2) the spontaneous carrier lifetime τ_s and photon lifetime τ_p are constant, 3) the gain coefficient is a linear function of injected electron density, 4) the only coupling between the laser modes is through the emission cross sections, and thus the envelope of the modes can be followed, and 5) the longitudinal mode structure due to Fabry-Perot effects can be recovered by multiplying the calculated envelope by the Fabry-Perot function. Under these assumptions, the equations for the rate of change of the injected electron density N and the photon flux per unit wavelength I inside the laser are[12]

$$\frac{dN}{dt} = \frac{J}{ed} - \frac{N}{\tau_s} - N \int \sigma(\lambda)\, I(t,\lambda) d\lambda \qquad 4\text{-}1$$

$$\frac{dI}{dt} = \frac{c}{n}\sigma(\lambda)\, NI(t,\lambda) + \frac{cg}{n\tau_s} E(\lambda)N - \frac{I(t,\lambda)}{\tau_p} \qquad 4\text{-}2$$

where J is the pump current density, d is the active region thickness and τ_s is the spontaneous carrier lifetime. $\sigma(\lambda)$ is the stimulated emission cross section given by

$$\sigma(\lambda) = \frac{\lambda^4 E(\lambda)}{8\pi c\, n^2 \tau_u}$$

where τ_u is the upper level lifetime, taken equal to τ_s, and $E(\lambda)$ is the spontaneous emission spectrum (all recombinations are assumed to produce radiative transitions, and thus $\int E(\lambda)\, d\lambda = 1$). g is the probability that a photon is emitted spontaneously into the mode, and τ_p is the photon lifetime, given by[11]

$$\tau_p = \frac{n}{c}\left[\frac{1}{L}\ell n\left(\frac{1}{R}\right) + \alpha\right]^{-1} \qquad 4\text{-}3$$

where L is the laser length, R is the facet reflectivity, and α is the bulk loss of the laser.

The origins of these terms can be explained as follows. In equation 4-1, the first term depends on the pumping current density applied to the laser, and increases the number of carriers. The second term is the decrease in the number of carriers due to spontaneous recombination (producing spontaneous pumping radiation). The third term is the decrease in carriers due to stimulated emission and is a function of the wavelength-dependant intensity multiplied by the stimulated emission cross section.

In equation (4-2), the first term is the increase in intensity due to stimulated emission. The second term is the increase in intensity due to spontaneous emission coupling into the lasing mode and the third term is the decrease in intensity due to loss out the mirrors and photon absorption.

The steady state solutions of the rate equations are obtained when dN/dt and dI/dt equal zero. Then (4-1) and (4-2) become

$$0 = \frac{J}{ed} - \frac{N_o}{\tau_s} - N_o \int \sigma(\lambda)\, I(\lambda)\, d\lambda \qquad 4\text{-}4$$

$$0 = \frac{c}{n}\sigma(\lambda)\, N_o\, I(\lambda) + \frac{cg}{n\tau_s} E(\lambda)\, N_o - \frac{I(\lambda)}{\tau_p} \qquad 4\text{-}5$$

For currents up to threshold, the photon flux will be approximately zero. Then equation (4-4) gives

$$N_o = \frac{J_{th}\,\tau_s}{ed} \qquad 4\text{-}6$$

For currents above threshold, if the spontaneous term in equation (4-5) is neglected (it will be much smaller than the stimulated term above threshold), equation (4-5) becomes

$$\frac{c}{n}\sigma(\lambda)\, N\, I(\lambda) = \frac{I(\lambda)}{\tau_p}$$

or

$$N_o = \frac{n}{c\,\sigma(\lambda)\,\tau_p} \qquad 4\text{-}7$$

Thus the carrier density above threshold is clamped at its threshold value, in the homogeneous broadening case.

An approximate analytic solution for the rate equations can be obtained for the case of small transient deviations ΔN and ΔI from the steady state value, produced by a step current function. The recombination rate terms are expanded about the equilibrium values N_o and I_o in the form

$$R = R_o + \frac{\partial R}{\partial N}\Delta N + \frac{\partial R}{\partial I}\Delta I \qquad 4\text{-}8$$

Thus equation (4-1) becomes

$$\frac{d}{dt}(\Delta N) = \frac{d}{dt}(N - N_o) = \frac{d}{dt}(N)$$

$$= \frac{J}{ed} - \frac{N_o}{\tau_s} - \frac{\Delta N}{\tau_s} - N_o A - A\Delta N$$

$$- BN\,\Delta I \qquad 4\text{-}9$$

where $A = \int \sigma(\lambda)\, I(\lambda) d\lambda$ and $B = \int \sigma(\lambda)\, d\lambda$

If the spontaneous emission term in equation (4-2) is neglected, it becomes in this small signal analysis

$$\frac{d}{dt}(\Delta I) = \frac{c}{n}\sigma(\lambda)\,[N_o\, I_o(\lambda) + I_o(\lambda)\,\Delta N + N_o\,\Delta I]$$

$$- \frac{I_o(\lambda)}{\tau_p} - \frac{\Delta I}{\tau_p} \qquad 4\text{-}10$$

Using the steady state solutions 4-4 and 4-5 derived earlier enables simplification to

$$\frac{d}{dt}(\Delta N) = -\frac{\Delta N}{\tau_s} - A\,\Delta N - BN\Delta I \qquad 4\text{-}11$$

$$\frac{d}{dt}(\Delta I) = \frac{c}{n}\sigma(\lambda)\, I_o(\lambda)\,\Delta N \qquad 4\text{-}12$$

Differentiating 4-11 and substituting from 4-12 gives

$$\frac{d^2}{dt^2}(\Delta N) + \left[\frac{1}{\tau_s} + A\right]\frac{d}{dt}(\Delta N) + BN\,\frac{c}{n}\sigma(\lambda)\, I_o(\lambda)\,\Delta N = 0 \qquad 4\text{-}13$$

as the differential equation for ΔN.

The equation for ΔI is obtained by solving 4-12 for ΔN and substituting in 4-11, giving

$$\frac{d^2}{dt^2}(\Delta I) + [\frac{1}{\tau} + A]\frac{d}{dt}(\Delta I) + BN\frac{c}{n}\sigma(\lambda)\, I_o(\lambda)\, \Delta I = 0 \qquad 4\text{-}14$$

These two equations are of the same form and have relaxation oscillation solutions

$$\Delta N = (\Delta N)_o \exp[-(\frac{1}{t_o} - iw_c)t] \qquad 4\text{-}15$$

$$\Delta I = (\Delta I)_o \exp[-(\frac{1}{t_o} - iw_c)t] \qquad 4\text{-}16$$

where $$\frac{1}{t_o} = \frac{1}{2}[\frac{1}{\tau_s} + A] \qquad 4\text{-}17$$

$$w = \frac{BNc}{n}\sigma(\lambda)\, I_o(\lambda) - \frac{1}{t_o^2}]^{1/2} \qquad 4\text{-}18$$

From the steady state solution 4-4,

$$\frac{J}{ed} = N_o \int \sigma(\lambda)\, I_o(\lambda)\, d\lambda + \frac{N_o}{\tau_s}$$

or $$\frac{1}{\tau_s} + A = \frac{1}{\tau_s} + \int \sigma(\lambda)\, I_o(\lambda)\, d\lambda = \frac{J}{edN_o} \qquad 4\text{-}19$$

Substituting this and equation 4-6 into 4-17 gives

$$t_o = \frac{2\,\tau_s\, J_{th}}{J} \qquad 4\text{-}20$$

Thus the oscillations in the photon and carrier populations die out on the order of the carrier lifetime, a few nanoseconds (figure 4-1).

To facilitate analysis of the relaxation oscillation frequency term, consider the case of the single mode laser, where I_o is

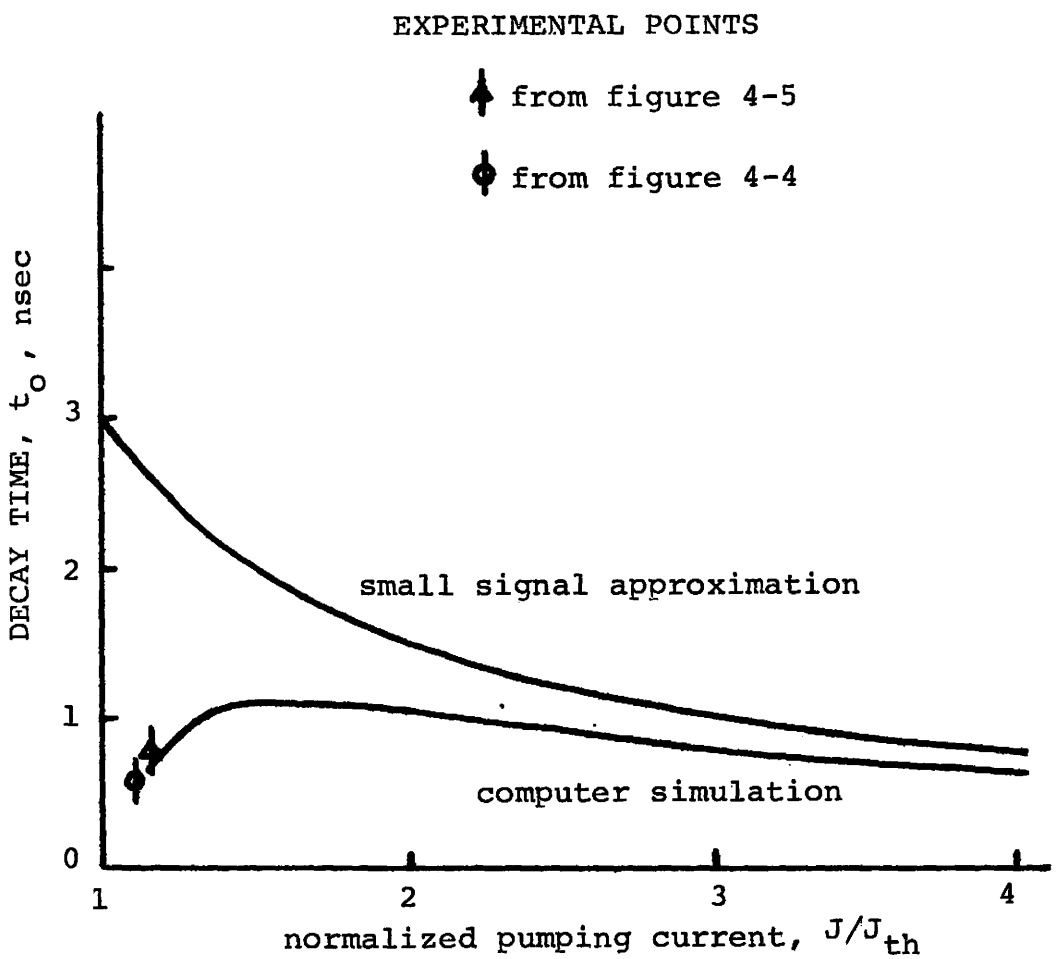

FIGURE 4-1 RELAXATION OSCILLATION DECAY TIME vs. PUMPING

independant of λ. Then from 4-4

$$\int \sigma(\lambda)\, I_o(\lambda)\, d\lambda = \frac{J}{edN_o} - \frac{1}{\tau_s} = I_o(\lambda) \int \sigma(\lambda)\, d\lambda = I_o(\lambda)\, B$$

Using this and equations 4-6 and 4-7 gives for the relaxation oscillation frequency

$$w = \left[\left(\frac{J}{edN_o} - \frac{1}{\tau_s}\right) \frac{1}{\tau_p} \frac{\tau_s}{\tau_s} - \frac{1}{t_o^2}\right]^{1/2}$$

$$= \left[\frac{1}{\tau_p\, \tau_s} \left(\frac{J}{J_{th}} - 1\right) - \frac{1}{t_o^2}\right]^{1/2} \qquad 4\text{-}21$$

Since $t_o \simeq 2$ nsec and $\tau_p = 1.47$ psec this becomes

$$w = 2\pi f = \left[\frac{1}{\tau_p\, \tau_s} \left(\frac{J}{J_{th}} - 1\right)\right]^{1/2} \qquad 4\text{-}22$$

This is converted to a pulse width and plotted in figure 4-2. Note that for a multimode laser, t_{osc} is a function of wavelength, and thus the various modes will oscillate at slightly different frequencies. Thus experimentally one would observe a smeared out set of damped oscillations as the modal oscillations get out of phase.

4.2 Experimental Relaxation Oscillations

Figures 4-3a) to d) show the laser diode response to a pumping current with 200 psec risetime and 600 psec FWHM. This pulse was not long enough to show the damping of the oscillations but the initial pulses were detected with a photodetector having a 60 psec FWHM response time. The laser pulse width was deconvoluted from the displayed width

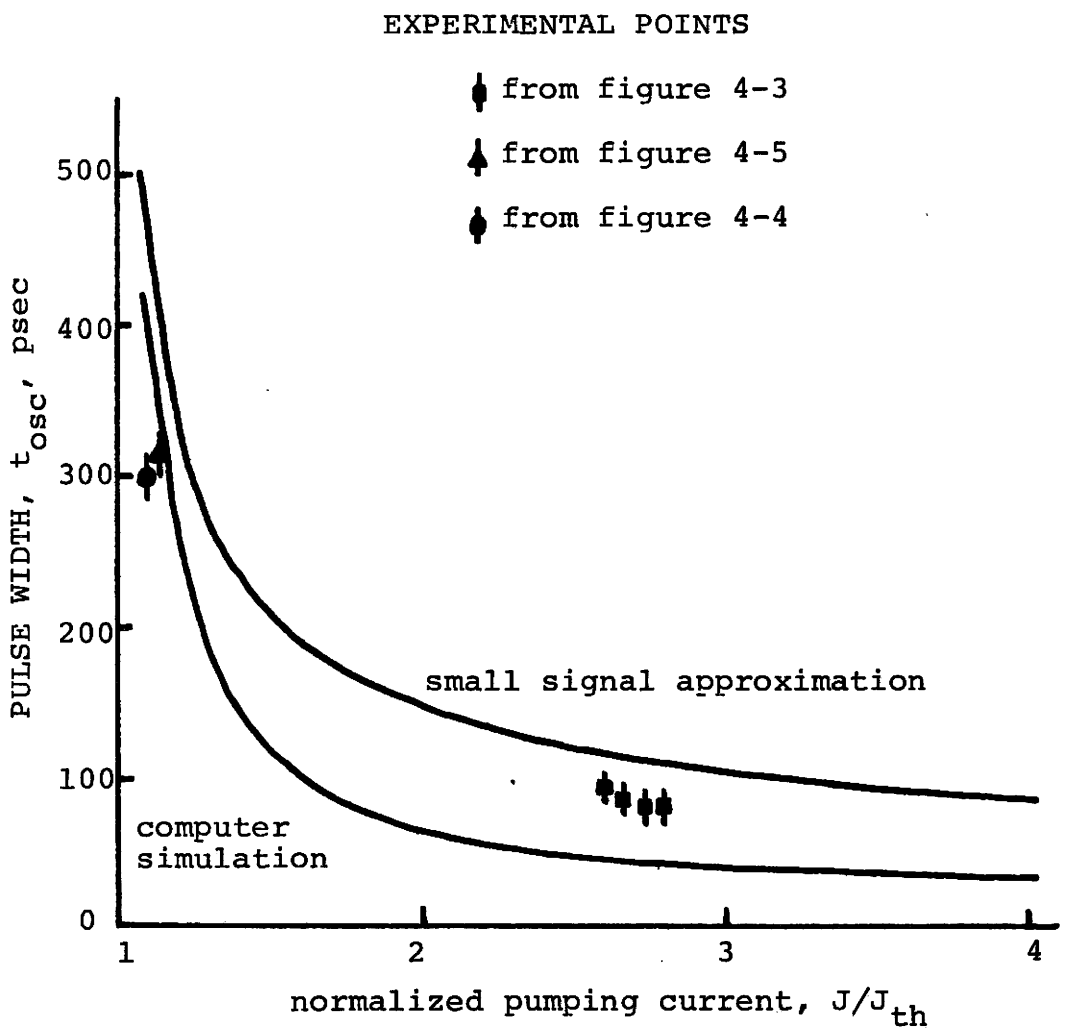

FIGURE 4-2 RELAXATION OSCILLATION PULSE WIDTH vs. PUMPING

FIGURE 4-3(a) RELAXATION OSCILLATIONS

$I = 2.60\ I_{th}$

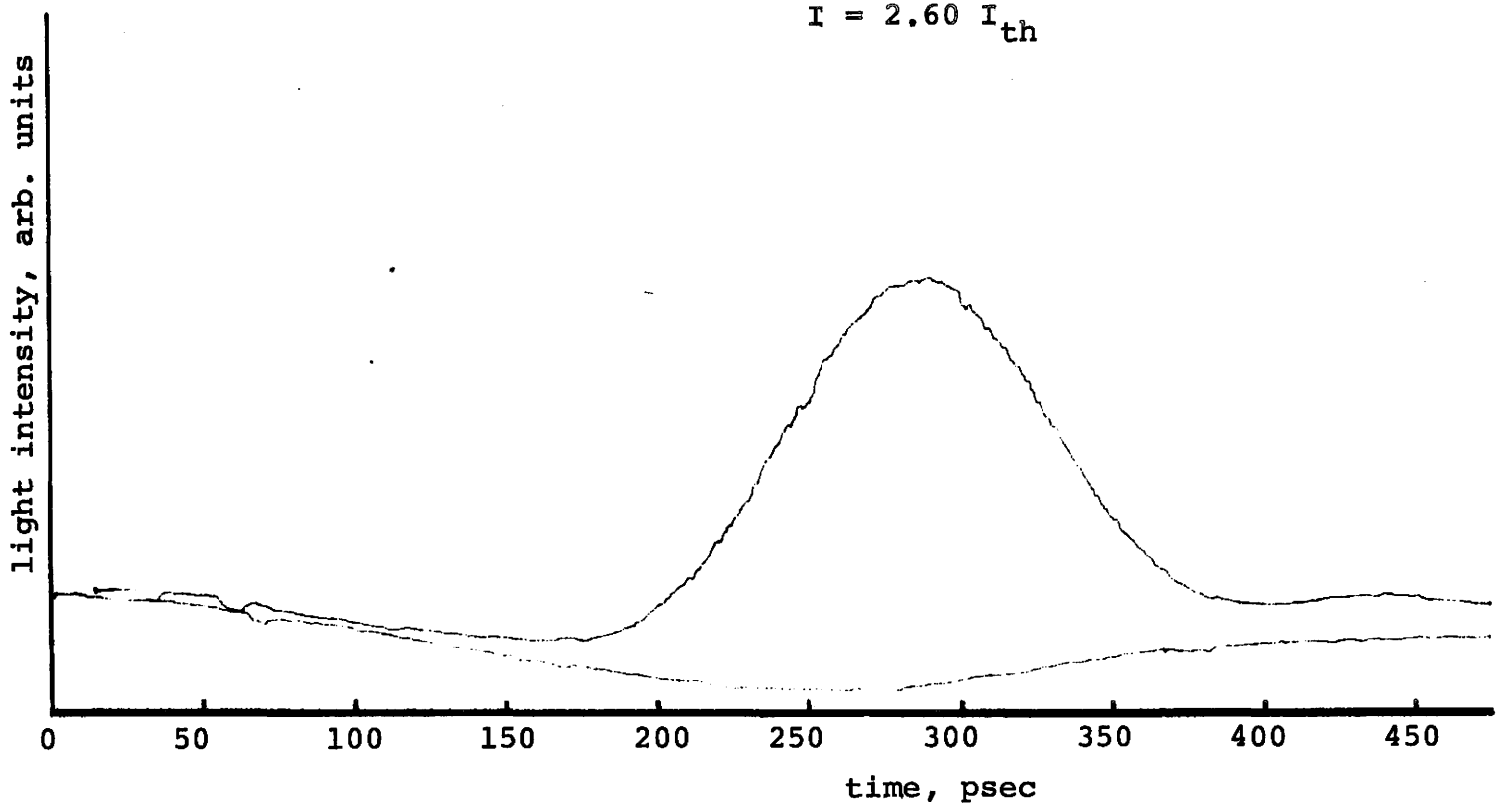

FIGURE 4-3(b) RELAXATION OSCILLATIONS

$I = 2.66\ I_{th}$

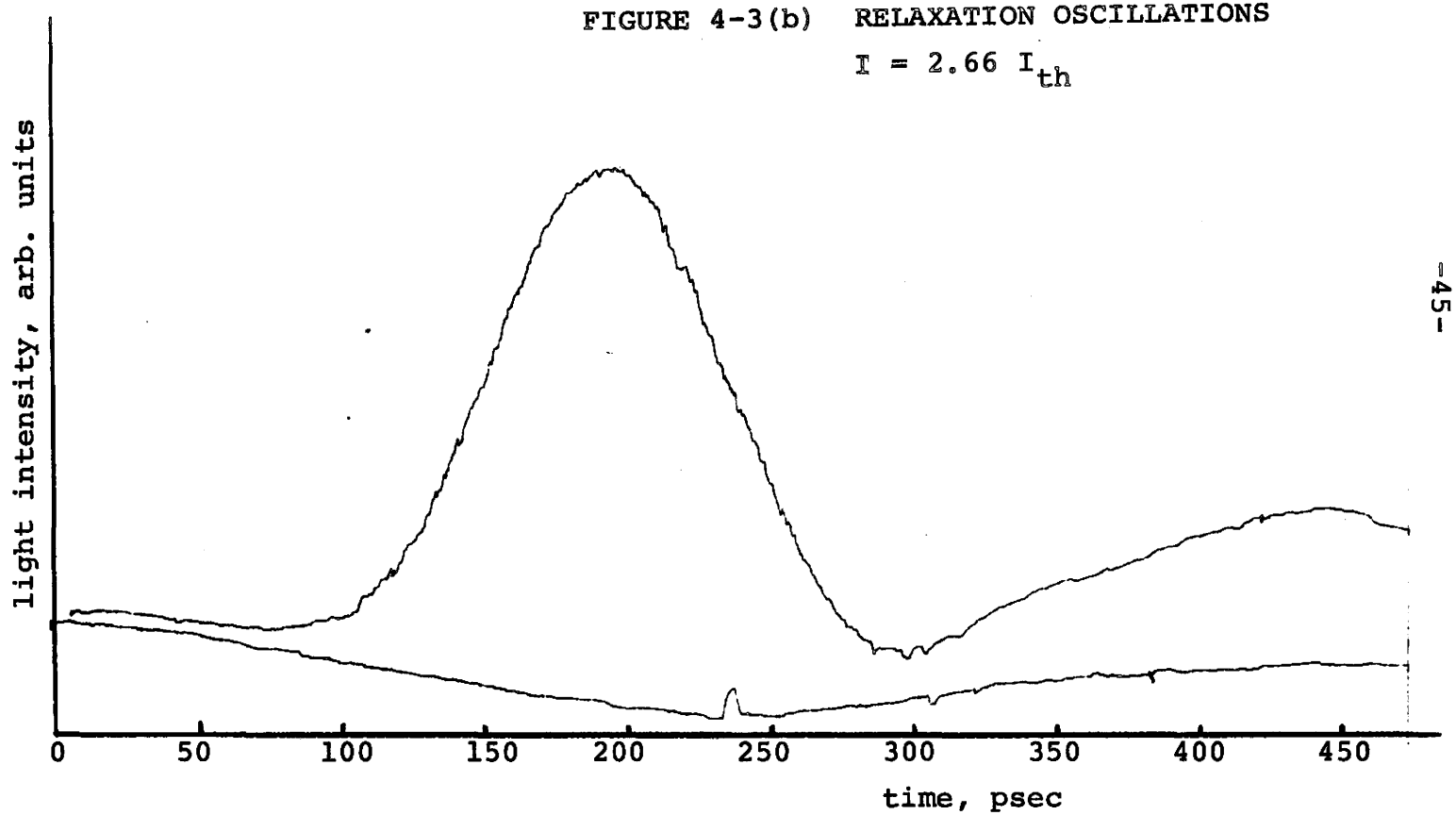

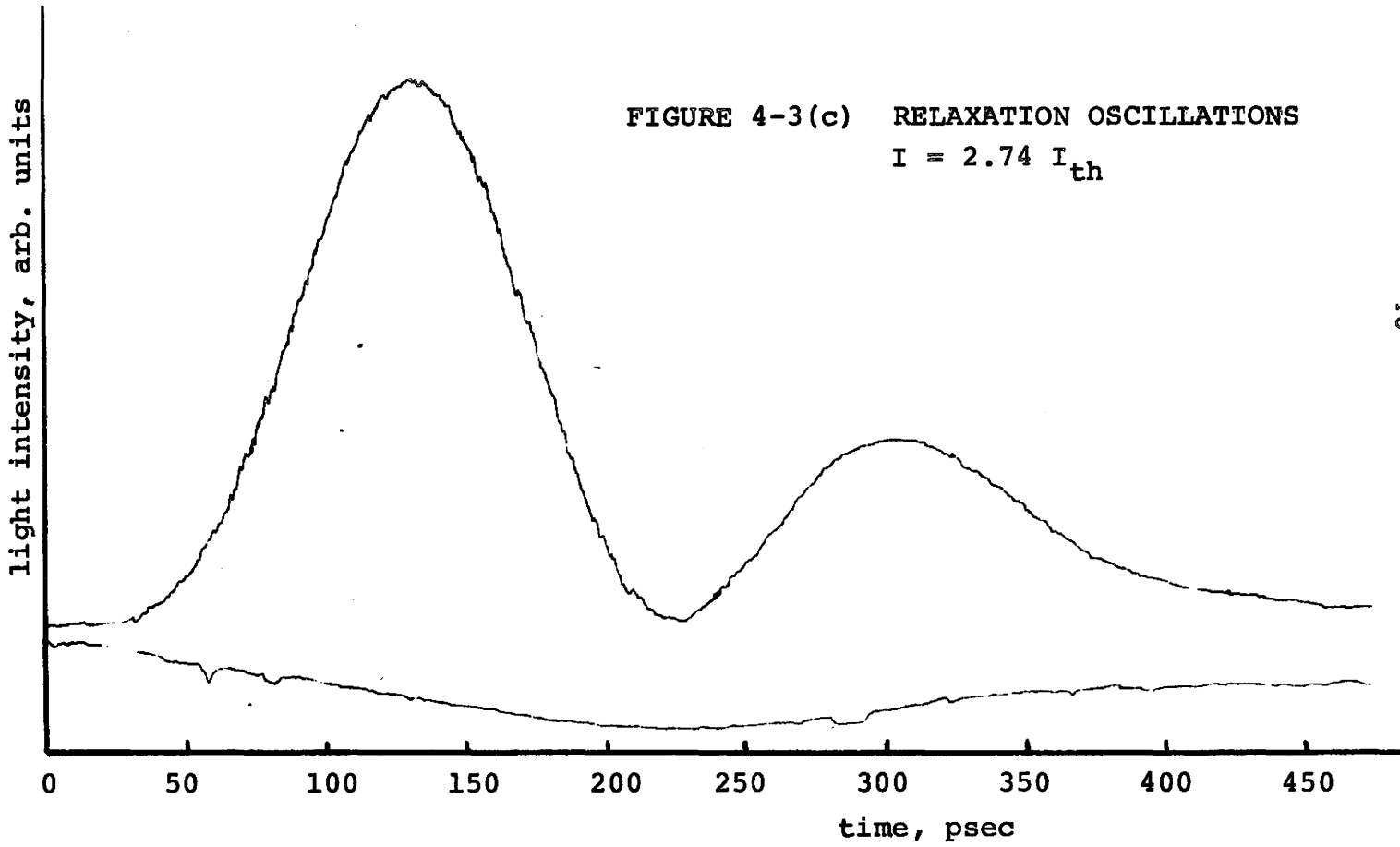

FIGURE 4-3(c) RELAXATION OSCILLATIONS
$I = 2.74\ I_{th}$

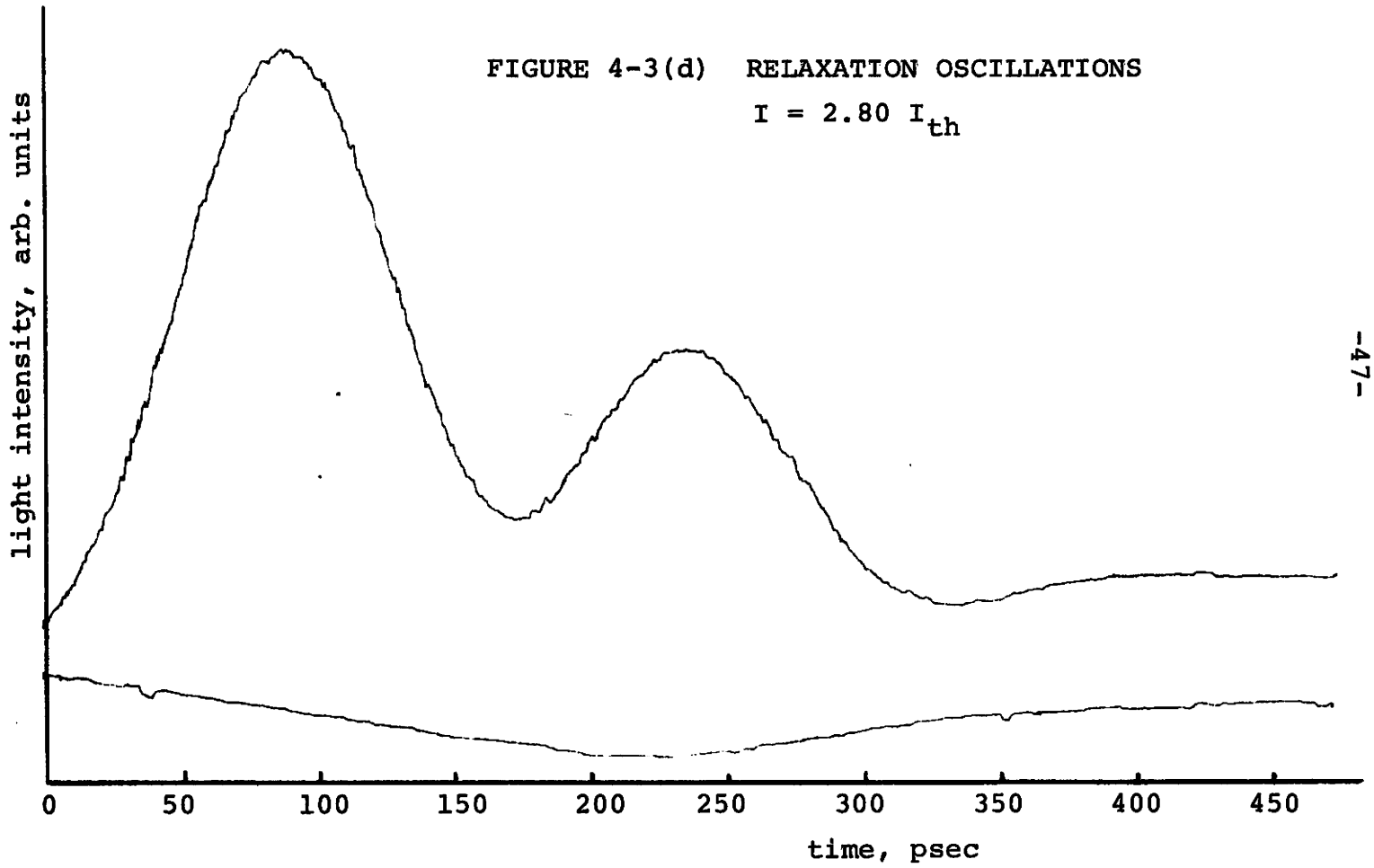

FIGURE 4-3(d) RELAXATION OSCILLATIONS

$I = 2.80\ I_{th}$

and plotted as a function of J/J_{th} in figure 4-2. It can be seen that there is fairly good agreement using this method.

In figures 4-3b) to d), a second light pulse is also visible. It would at first appear that this is the second oscillation of the light pulse. However the frequency obtained from this pulse to pulse spacing increases much more rapidly than the predicted values or the values obtained from the pulse width. Thus this second pulse is probably the initial pulse from a different mode in the laser. The width of this pulse is decreasing with increasing current, indicating a separate mode (either spatially separate or a different wavelength) which has a higher threshold than the first.

Figures 4-4 and 4-5 show relaxation oscillations obtained with mild pumping (1.1 and 1.15 I_{th}) and longer current pulses. The detector used here had a FWHM of 210 psec and the deconvoluted pulse widths agree fairly well with the small signal approximation (figure 4-2). The 1/e decay times are about 1.5 nsec, which is on the order of the predicted value (figure 4-1).

With the short and/or low amplitude pulses used in these pulse situations, it is fairly easy to produce one dominant mode, or to differentiate between modes. With longer pulses and harder pumping, the wavelength effects of the rate equations become more pronounced and the linear approximation is not good enough. A computer program has been written by John Goodwin[13] which numerically solves the rate equations 4-1 and 4-2 and gives intensity, population inversion, and spectral width as a function of time. The predicted relaxation oscillation pulse

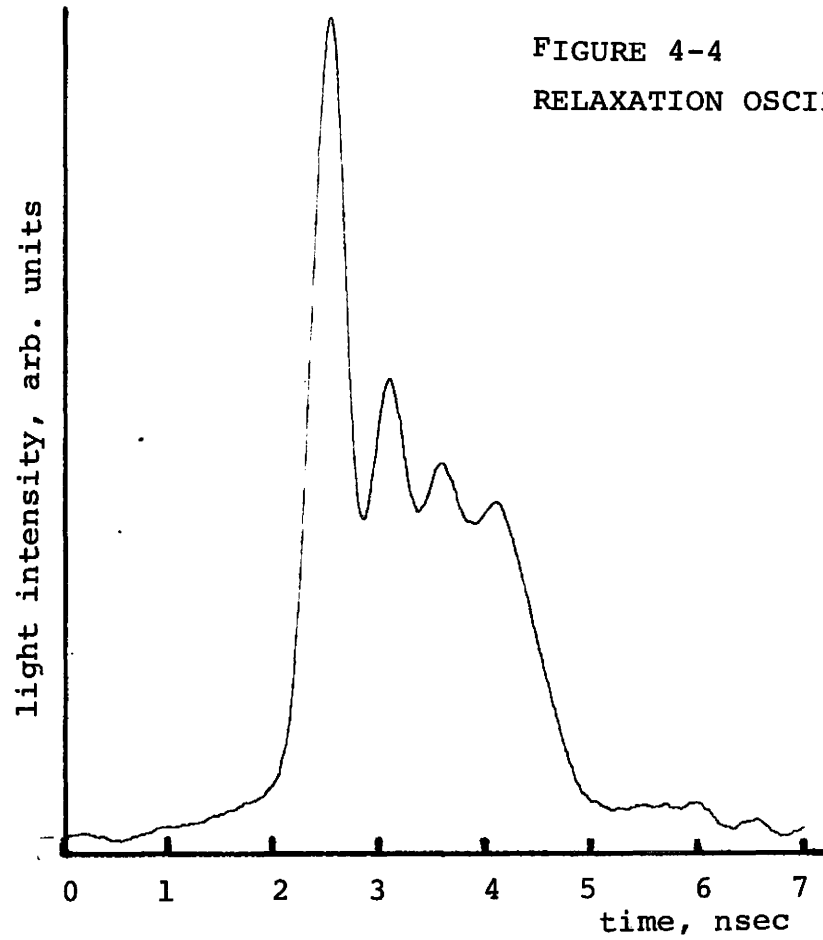

FIGURE 4-4

RELAXATION OSCILLATIONS, $I=1.1\ I_{th}$

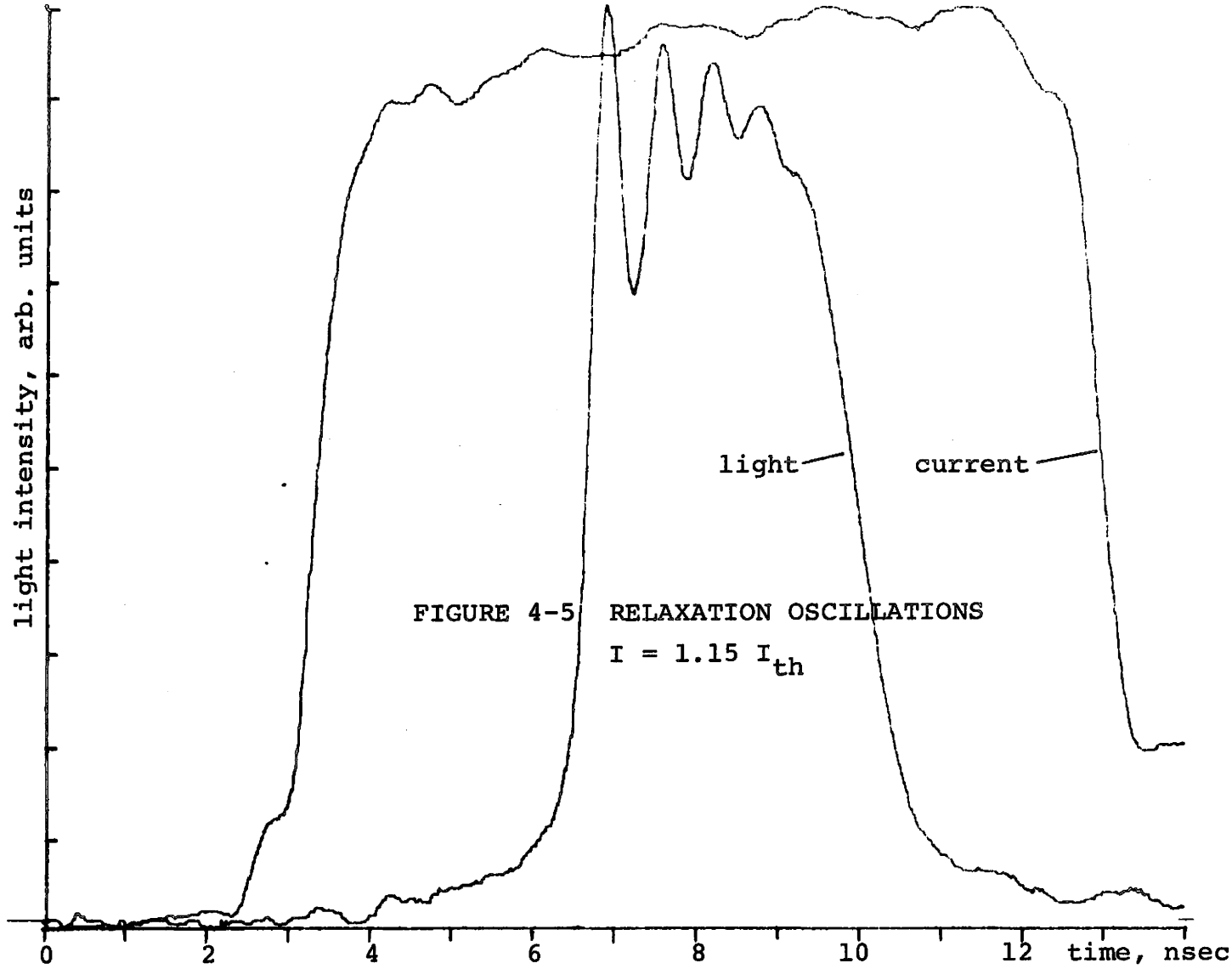

FIGURE 4-5 RELAXATION OSCILLATIONS

$I = 1.15\ I_{th}$

widths are shown in figure 4-2, and show good agreement with the experimental and small signal values. For low pumping currents, where the relaxation oscillations had a clearly decaying envelope, there was much better agreement with the simulation than with the small signal analysis. It is informative to note that the small signal solution ignored the spontaneous light term in equation 4-2. The simulations have shown that this term has the effect of damping the relaxation oscillations. Thus, as was observed experimentally, the simulations predict a much shorter decay time for low pumping. Note that for high pumping, where light output is higher and the spontaneous term is a smaller fraction, the two solutions converge.

The great value of the program is for low to moderate current pumping, where interaction between the modes due to the wavelength dependance of the emission cross sections is important. The model does not take into account the interaction of modes due to spatial hole burning and similar effects, which become important at high pumping levels.

Figure 4-6 shows a simulation of the experimental situation in figure 4-7. Using typical and measured parameters for the laser diode used, there is good quantitative agreement of frequency and decay parameters of the oscillations. Fitting of the decay parameters was done mainly using the spontaneous coupling coefficient g in equation 4-2.

For higher pumping currents (2 I_{th}), it appears that mode competition not allowed for in these two models takes over. For

FIGURE 4-6 SIMULATED RELAXATION OSCILLATIONS

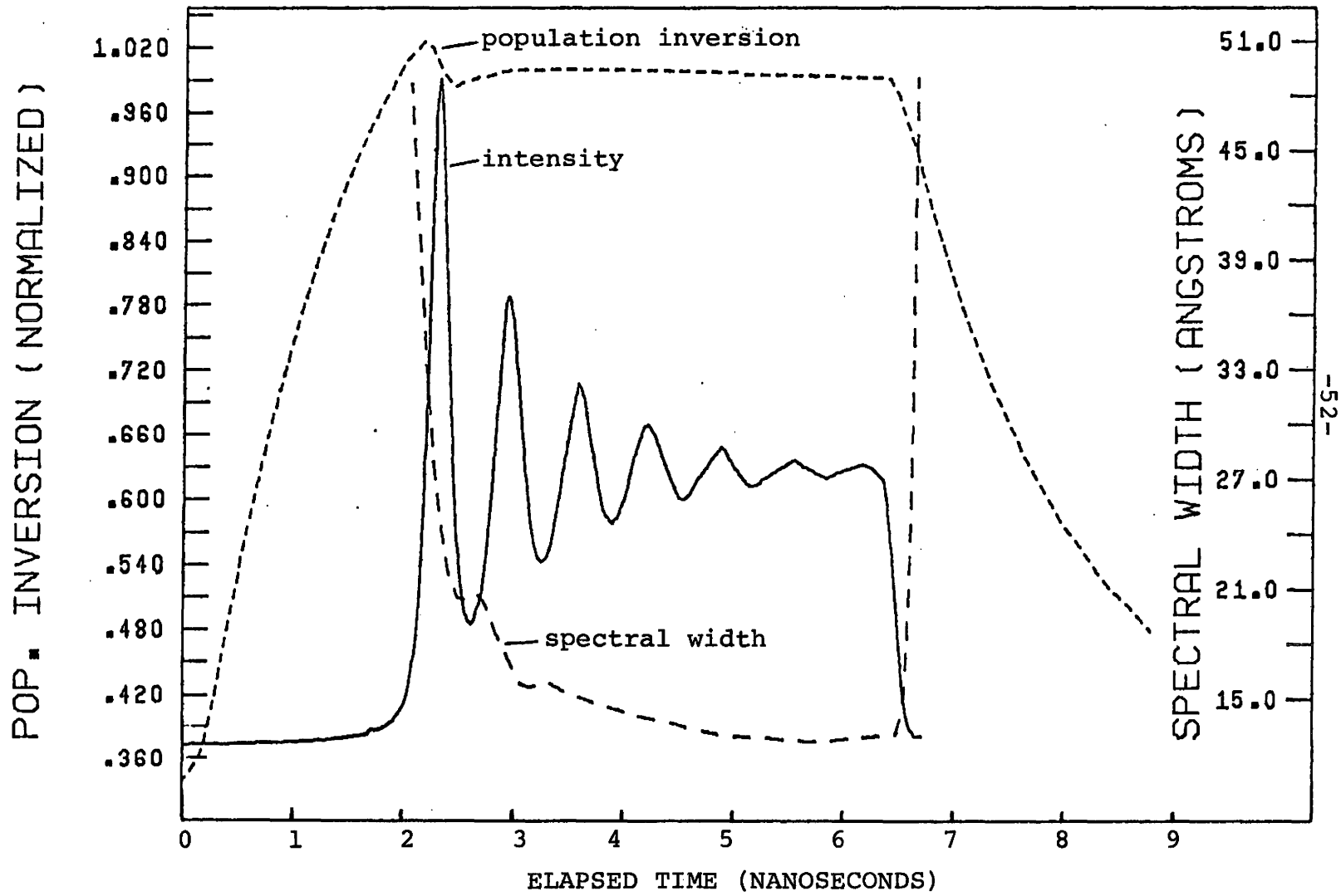

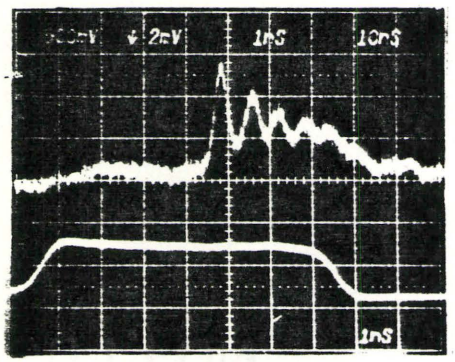

FIGURE 4-7 RELAXATION OSCILLATIONS

upper: light pulse
lower: current pulse

(This pumping is simulated in fig. 4-6)

example, in figure 4-8 the pumping current was 1.9 I_{th}. The predicted pulse width for this pumping is (figure 4-2) about 150 psec. The observed width was about 500 psec, although the decay time t_o was close to predicted (figure 4-1). As the current was increased slightly, to 2.2 I_{th} (figure 4-9) and 2.3 I_{th} (figure 4-10), the pulse shape changes dramatically, and the models are obviously not adequate to describe the dynamic behaviour.

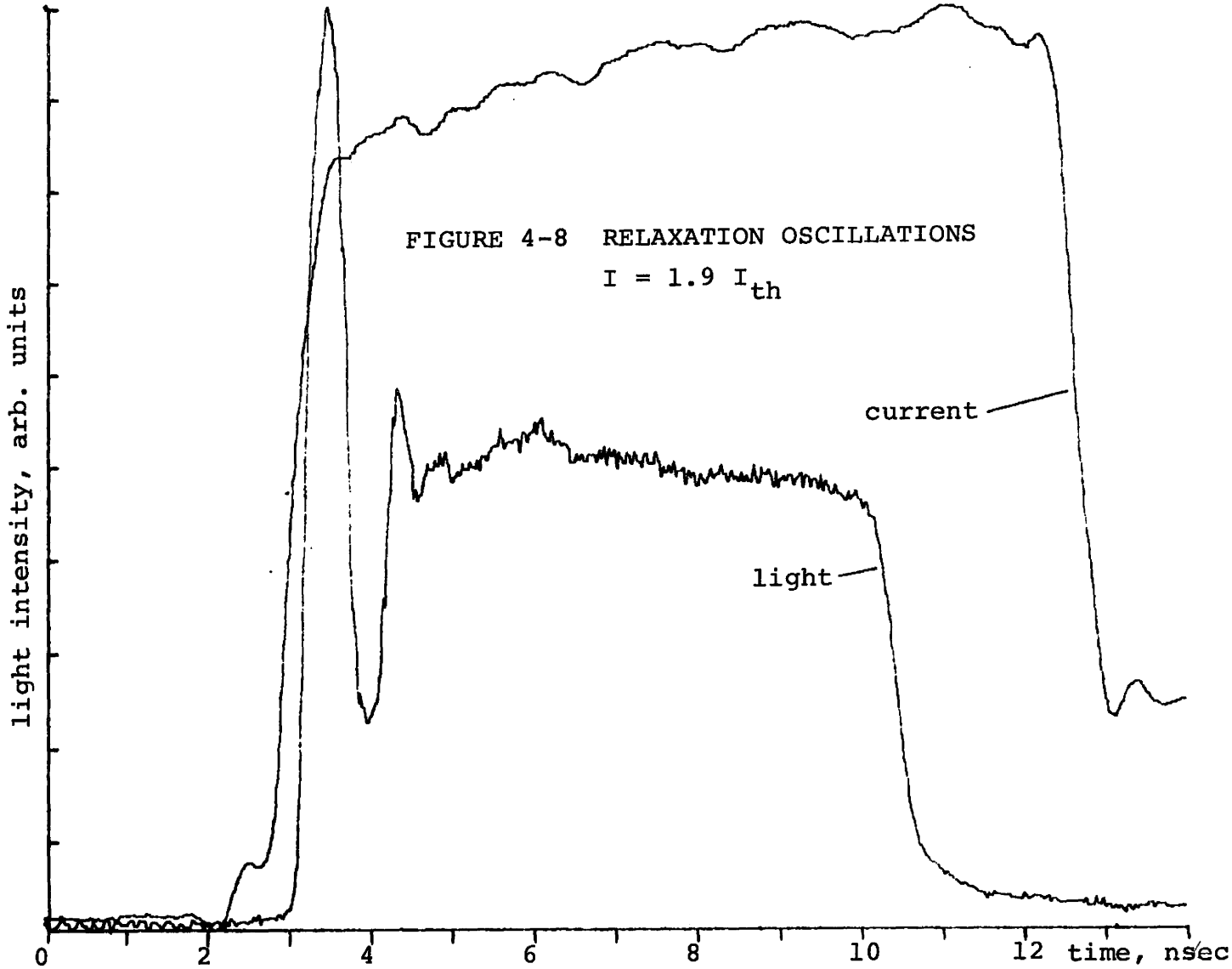

FIGURE 4-8 RELAXATION OSCILLATIONS
$I = 1.9\ I_{th}$

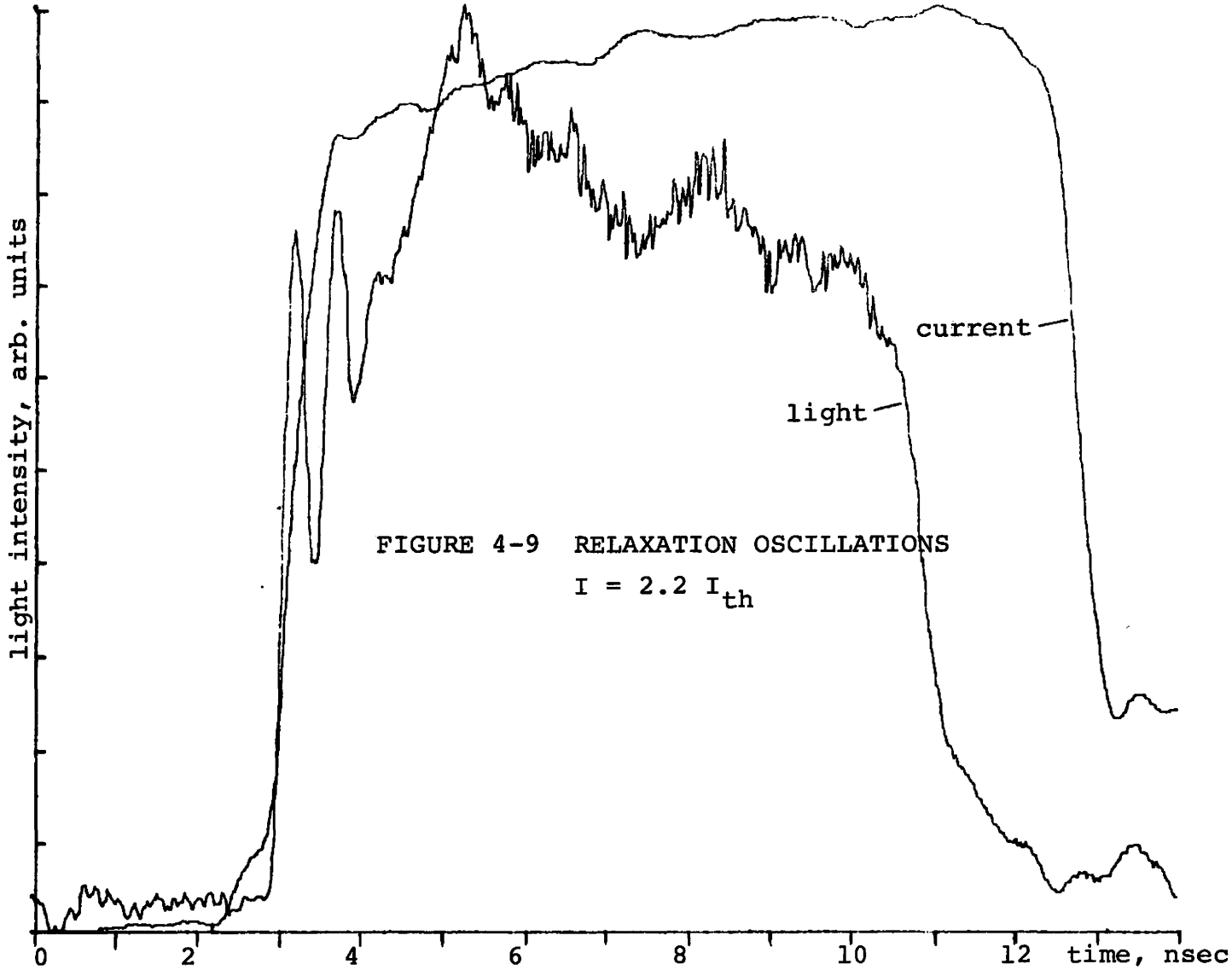

FIGURE 4-9 RELAXATION OSCILLATIONS
$I = 2.2\ I_{th}$

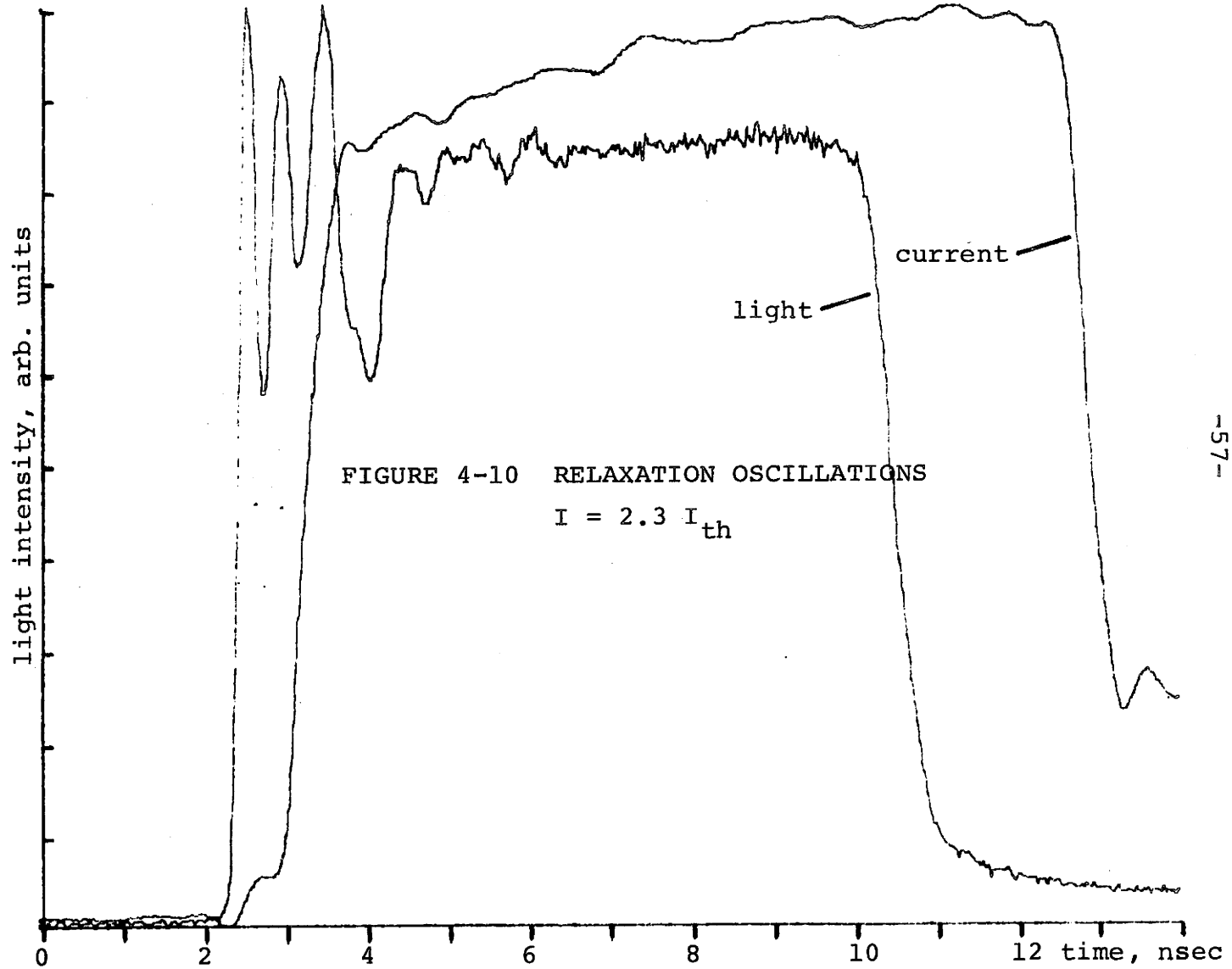

FIGURE 4-10 RELAXATION OSCILLATIONS

$I = 2.3\ I_{th}$

5 EXTERNAL CAVITY

5.1 d.c. changes

To describe the d.c. changes in laser emission of a diode laser in an external cavity, the method of a composite reflectivity can be used. The reflectivities of the laser diode face and the external cavity are combined into a single reflectivity coefficient (fig 5-1). In general, this coefficient will be wavelength dependant due to the phase delay $\phi=2\pi nL/\lambda$ in the external cavity length L. For typical cavities used here ($\simeq$10 cm) however, the mode spacing of the external cavity is much less than the amplification profile of the laser and the phase retardation of the cavity may be ignored in calculating the threshold current.

At lasing threshold, the optical gain per unit length g_{th} equals the optical loss per unit length

$$\Gamma g_{th} = \alpha - \frac{1}{L_d} \ell n \sqrt{R_1 R_2} \qquad 5\text{-}1$$

where Γ is the fraction of light which is amplified, α is the absorption per unit length in the laser, L_d is the diode length, and R_1 and R_2 are the laser mirror reflectivities. The gain function can be approximated by a linear dependance on current density

$$g = \beta (j - j_o) \qquad 5\text{-}2$$

where β and j_o depend on material properties.

Thus the threshold current density is

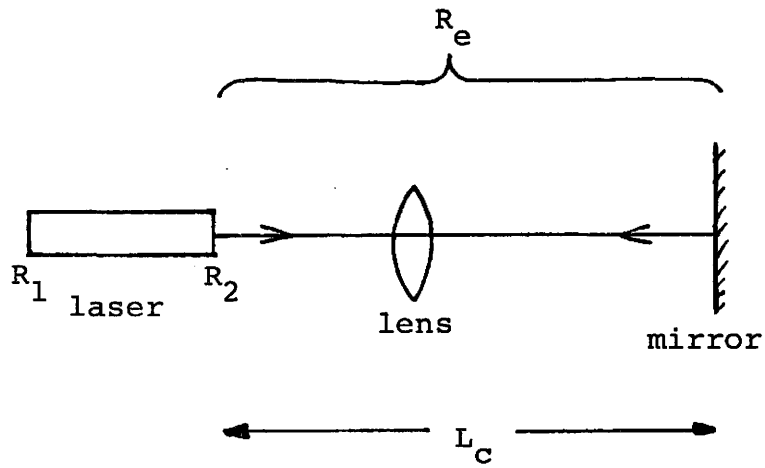

FIGURE 5-1 EXTERNAL CAVITY

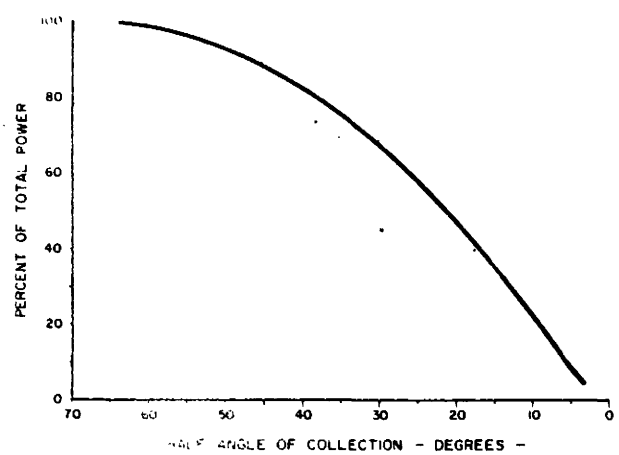

FIGURE5-2 POWER COLLECTED vs. COLLECTION ANGLE

$$j_{th} = \frac{1}{\beta\Gamma}\left[\alpha - \frac{1}{L_d} \ln \sqrt{R_1 R_2}\right] + j_o \qquad 5\text{-}3$$

For an isolated laser diode, $R_1 = R_2 = 32\%$ from the cleaved end faces. For the diode with an external cavity of effective reflectivity $R_2 = R_e$, there will be a change in threshold

$$\frac{\Delta j_{th}}{j_{thi}} = \frac{j_{thi} - j_{thc}}{j_{thi}} = \frac{\ln \sqrt{R_1 R_e} - \ln \sqrt{R_1 R_2}}{L_d\left[\left(\alpha - \frac{1}{L_d} \ln \sqrt{R_1 R_2}\right) + j_o \beta \Gamma\right]}$$

$$= \frac{\ln \sqrt{R_e/R_2}}{L_d\alpha - \ln \sqrt{R_1 R_2} + j_o \beta \Gamma L_d} \qquad 5\text{-}4$$

Since the diode facet reflectivity R_1 is in general different from the effective reflectivity R_e, the power output is different from the two ends of the laser system. The threshold change is a useful measure of the external cavity effect.

As discussed in section 2.5, the best external cavity effects (i.e. largest threshold changes) were obtained when a microscope objective was used to collimate the laser light. Some effects were obtained with the 1" diameter compound lens system; with careful alignment and the 100% mirror/beam splitter combination, a c.w. threshold drop of $\simeq$ 4 mA was observed with laser diode #2 using a compound 25 mm diameter, 22 mm focal length lens. This lens consisted of two plano convex lenses and had an effective collection half angle of 25°. When a 10X microscope objective, which had a collection half angle of 15° was used with the same setup, the c.w. threshold change with

cavity was approximately 10 mA (fig 5-3). Thus although the compound lens system collected 1.7 times as much light (fig 5-2, 57% compared to 33%), the aberrations in the compound lens system offset this advantage. Since the d.c. threshold current of this laser diode was 135 mA, the 10 mA change implied (equation 5-4) that the external cavity had an effective reflection coefficient of approximately 44%.

5.2 Spatial Emission Changes

Another cavity effect which was observed was the control of the laser filamentary action by the feedback light. Due to local defects such as non-uniform dopant density, precipitates, and non radiative centers, the diode laser output is not uniform across the active area, but occurs in 'filaments'. The near field pattern of laser #1 had two main lasing areas, one brighter than the other. The relative intensities could be changed by focussing the reflected spot on one of the areas, decreasing the effective cavity loss for that area and increasing the optical output.

5.3 Dynamic Effects

The dynamic effects of the external cavity can be predicted by treating it as a time delay unit and adding an extra term in the rate equations which corresponds to the photon number at an earlier time $t-t_c$ where $t_c = 2L/c$. If the finesse of the external cavity is low, as in most cases, this approach is valid[14] and rate equation 4-1 becomes

FIGURE 5-3 L vs. i, EXTERNAL CAVITY

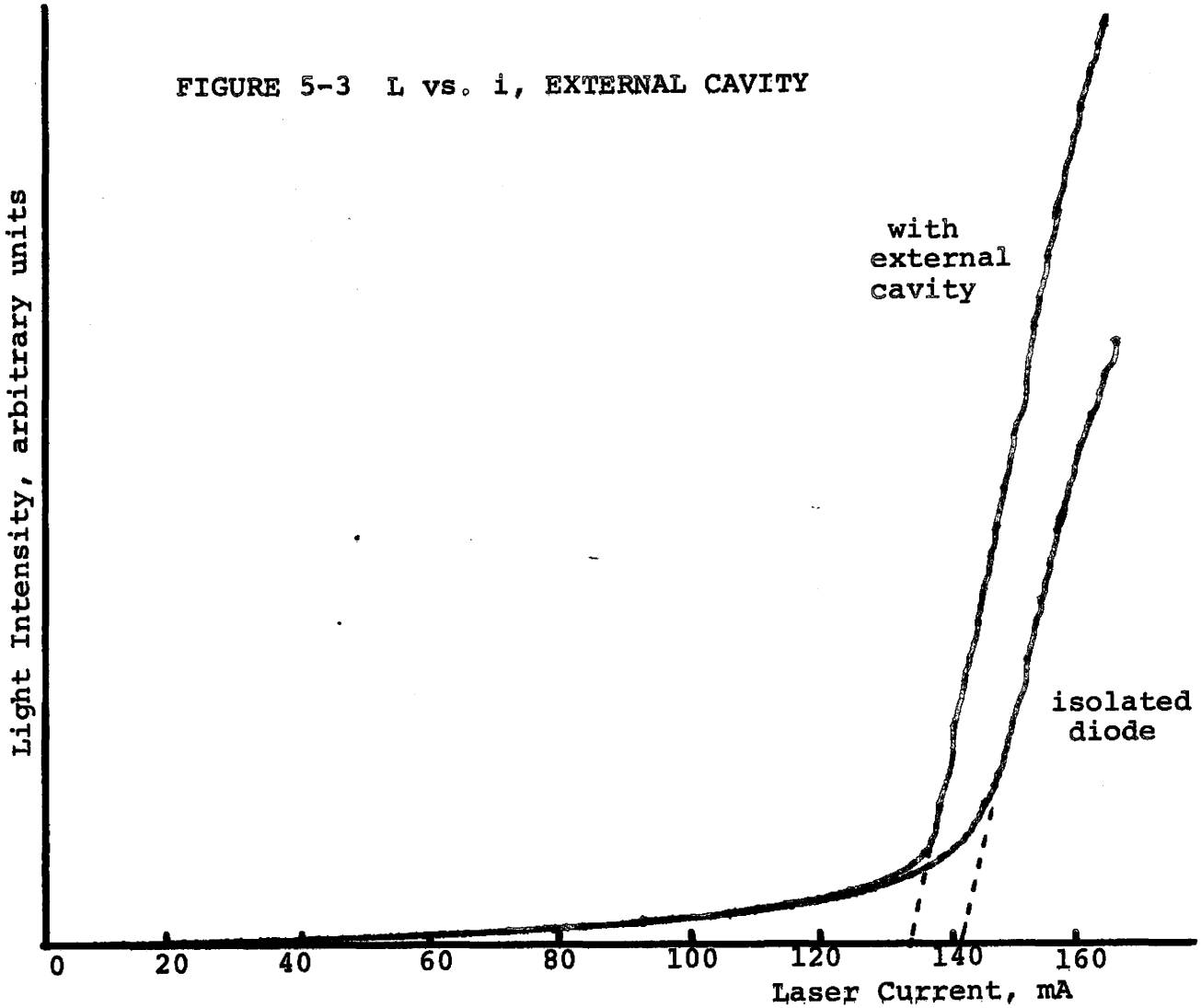

$$\frac{dI}{dt} = \frac{c}{n}\,\sigma(\lambda)\,NI(t,\lambda) + \frac{cg}{n\tau_s}\,E(\lambda)\,N - \frac{I(t,\lambda)}{\tau_p}$$

$$+ k\,I(t - t_c, \lambda) \qquad 5\text{-}5$$

where k is a coupling factor. The value of k for a particular experimental situation can be obtained from the measured d.c. threshold change. The threshold condition applied to equation 5-5 gives

$$\frac{c}{n}\,\sigma(\lambda)\,N_{thc} - \frac{1}{\tau_p} + k = 0$$

or
$$N_{thc} = \frac{1/\tau_p - k}{c\,\sigma(\lambda)/n} \qquad 5\text{-}6$$

The case of k = 0 gives the threshold condition without the cavity, and thus the change in threshold current is related to k by

$$\frac{\Delta i_{th}}{i_{th}} = \frac{i_{th} - i_{thc}}{i_{th}} = \frac{N_{th} - N_{thc}}{N_{th}}$$

$$= \frac{1/\tau_p - (1/\tau_p - k)}{1/\tau_p} = \tau_p k \qquad 5\text{-}7$$

The external cavity rate equations have also been simulated by John Goodwin[13]. Figure 5-4 shows typical laser diode relaxation oscillations without the external cavity, and figure 5-5 and 5-6 show the enhanced relaxation oscillations for two cavity lengths. For figures 5-5 and 5-6, the coupling coefficient and cavity lengths are comparable to the experimental values.

The experimental effects of the external cavity on the relaxation oscillations can be seen in figures 5-7 to 5-9. Although the percentage

FIGURE 5-4 SIMULATED RELAXATION OSCILLATIONS, NO EXTERNAL CAVITY

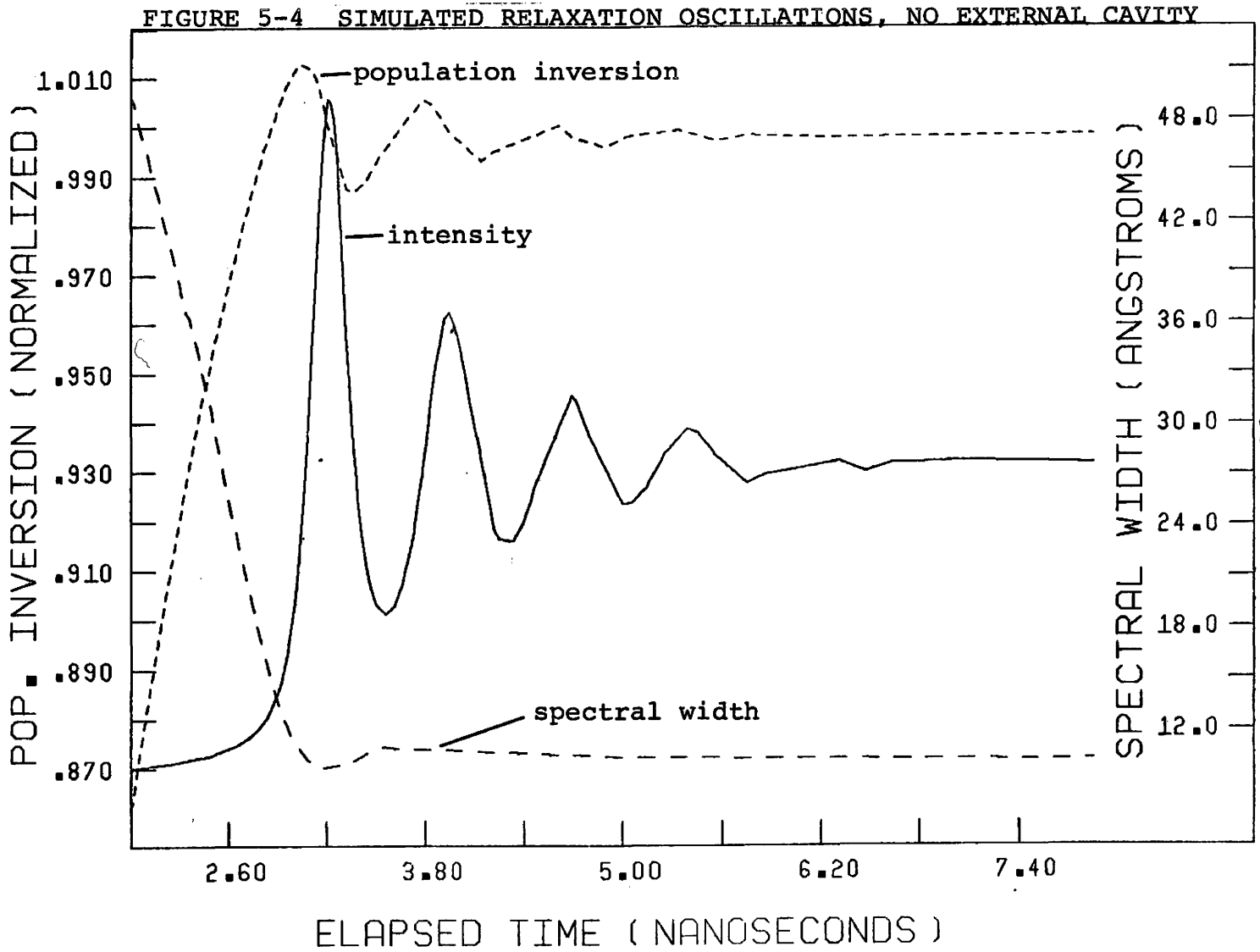

FIGURE 5-5 SIMULATED RELAXATION OSCILLATIONS, EXTERNAL CAVITY L_c#2

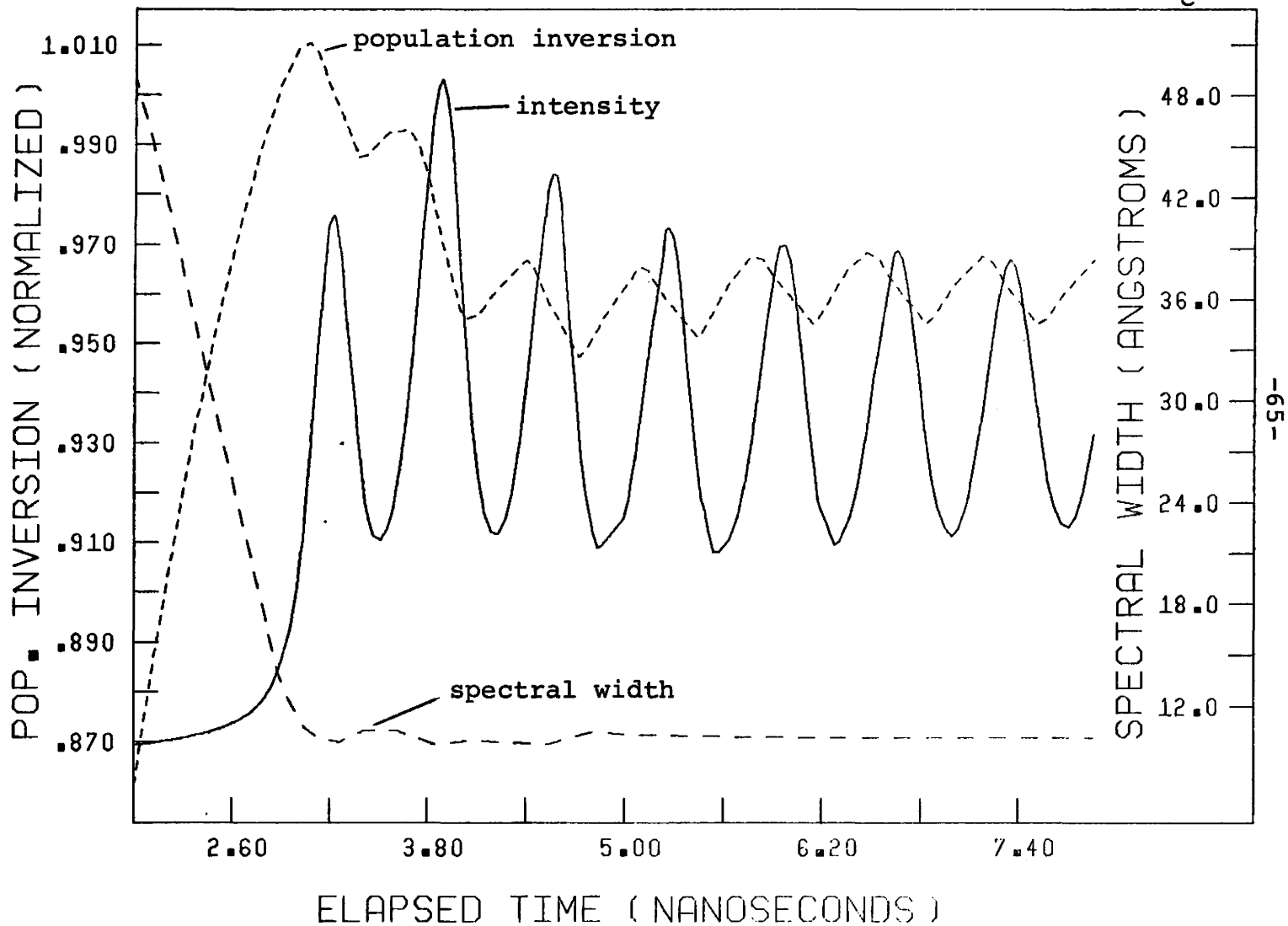

FIGURE 5-6 SIMULATED RELAXATION OSCILLATIONS, EXTERNAL CAVITY #2

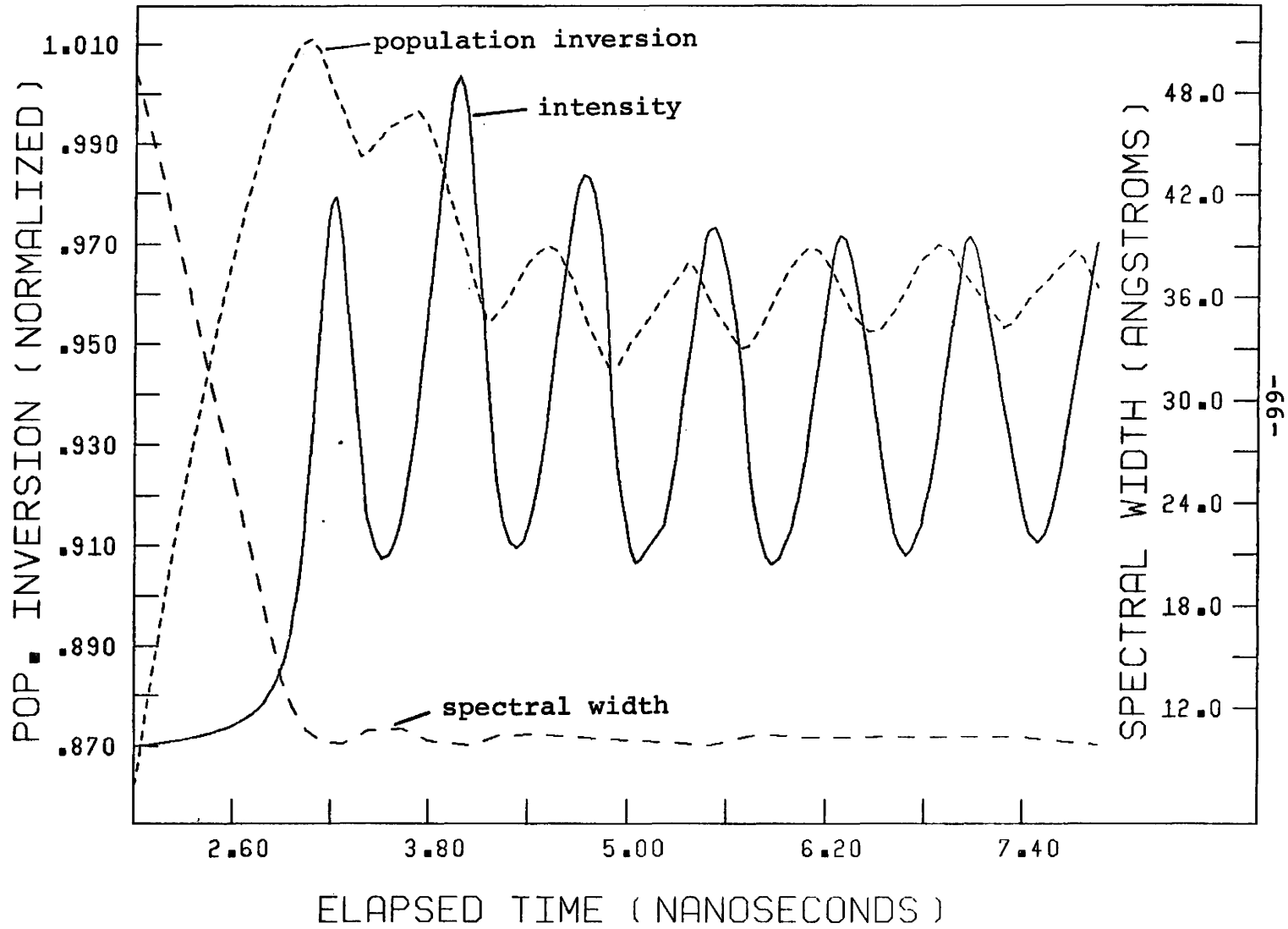

FIGURE 5-7 RELAXATION OSCILLATIONS, L_c = 14.0 cm

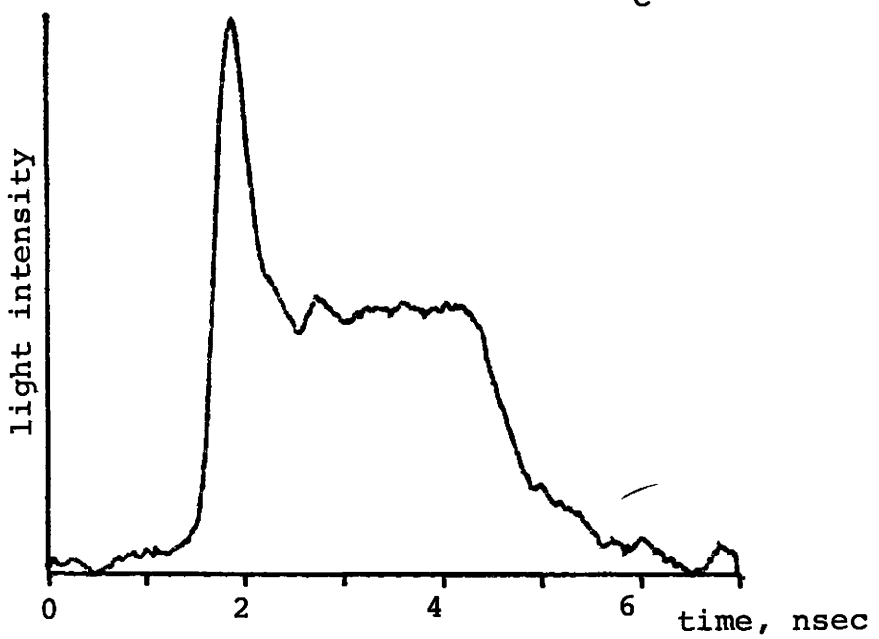

(a) without cavity

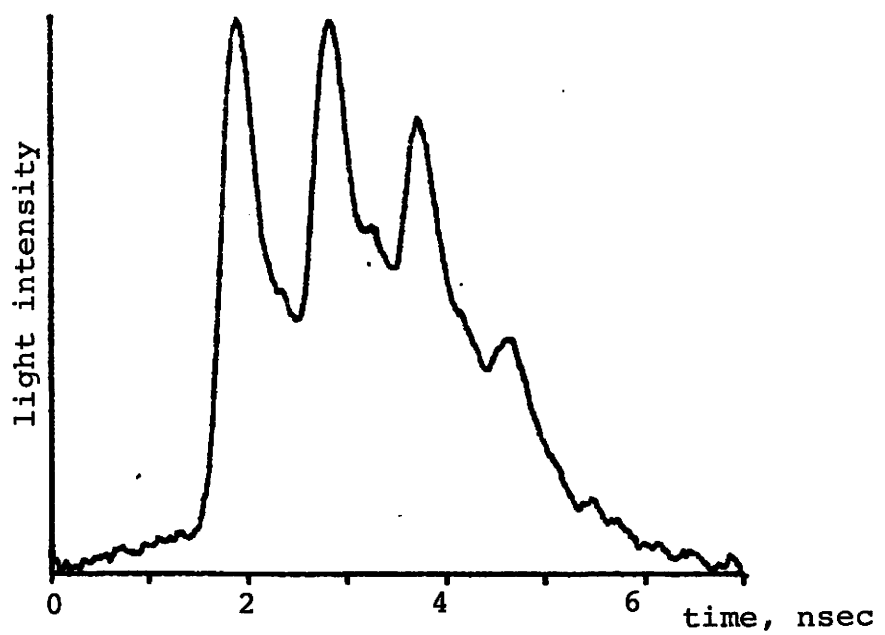

(b) with cavity

FIGURE 5-8 RELAXATION OSCILLATIONS, L_c = 14.0 cm

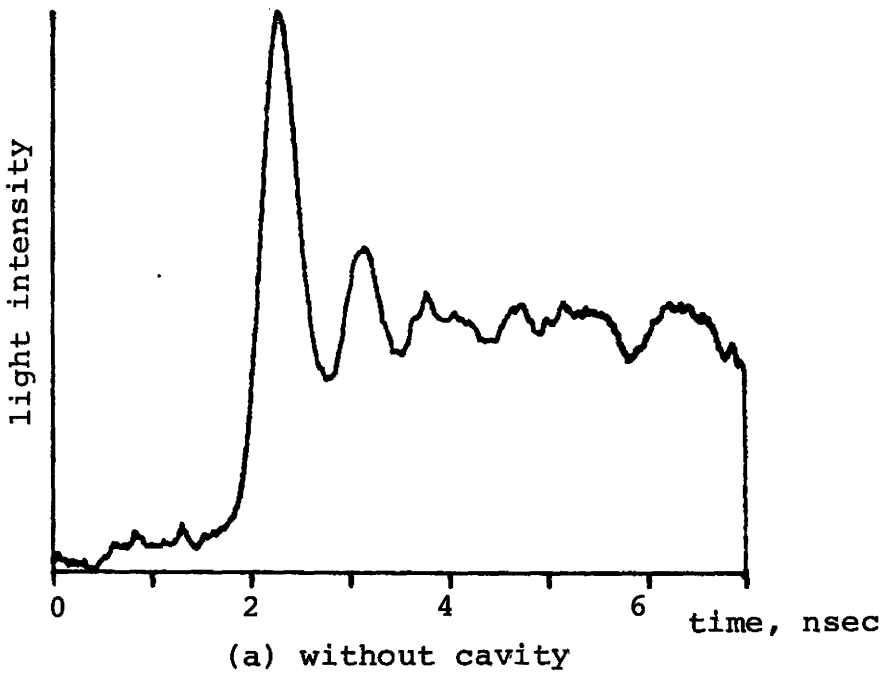

(a) without cavity

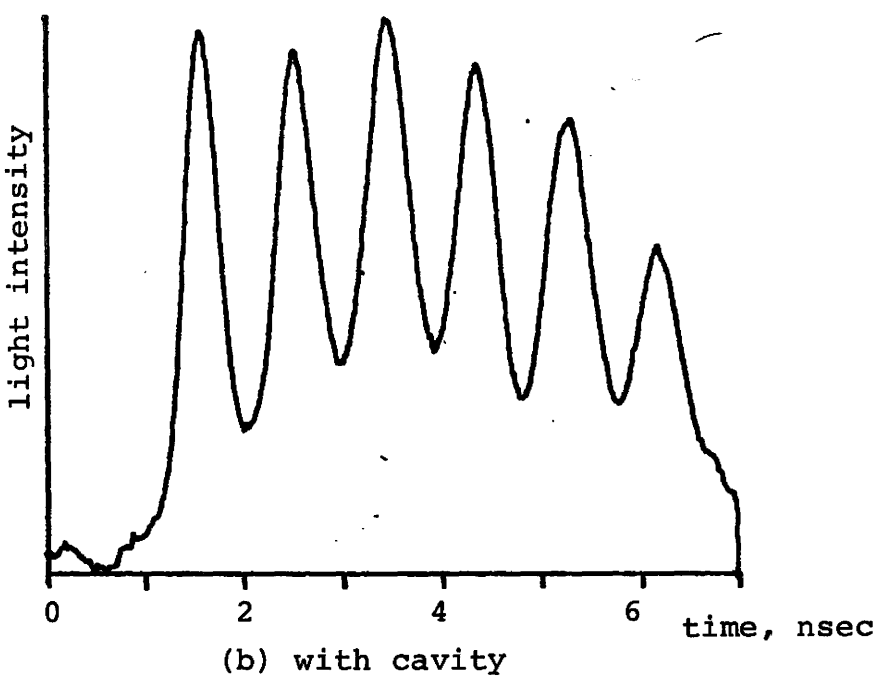

(b) with cavity

FIGURE 5-9 RELAXATION OSCILLATIONS, L_c = 11.4 cm

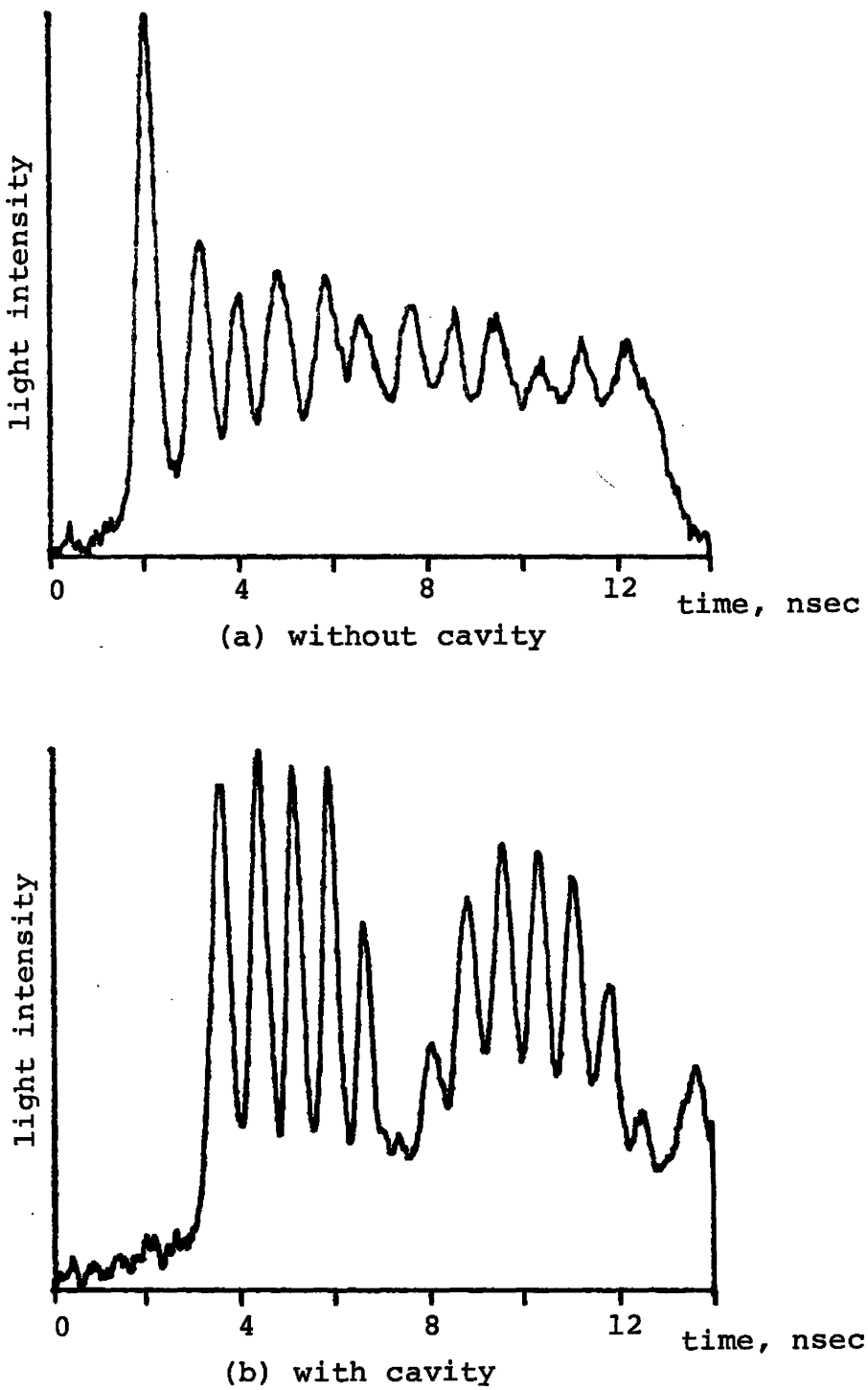

of feedback was not all that large, there was a marked effect on the laser behaviour. The greatest enhancement of the relaxation oscillations occured for round trip cavity times which were slightly smaller than the natural oscillation time. That this situation gives the maximum short term enhancement can be explained by observing that the population inversion and thus the gain will be a maximum before the peak of the light pulse (figure 5-4). It is this phase difference which produces the relaxation oscillations in the first place.

It was observed that the cavity length could be varied over a fairly wide range with relatively little effect on the amplitude of the oscillations. This is probably due to the small feedback coefficient, since other workers have seen very strong cavity length dependance. This hypothesis is backed by the computer simulations, which showed negligible difference in enhancement over a 25% range of cavity lengths at this coupling coefficient (figures 5-5, 5-6). However for coupling coefficients 50% larger there was a pronounced length dependance in the simulations.

The enhanced relaxation oscillation period was dependant on cavity length, as is shown in figure 5-10. Over the range of cavity lengths shown, where strong enhancement was observed, the period of the oscillations was pulled by the cavity to the external round trip time, although this varied by $\pm$ 15% from the natural relaxation oscillation period (figure 5-7a). (This effect was also observed with the computer simulations figures 5-5 and 5-6). Thus although for this mild coupling case there was no strong resonance between the cavity and the natural

FIGURE 5-10 CAVITY OSCILLATION PERIOD vs. CAVITY LENGTH

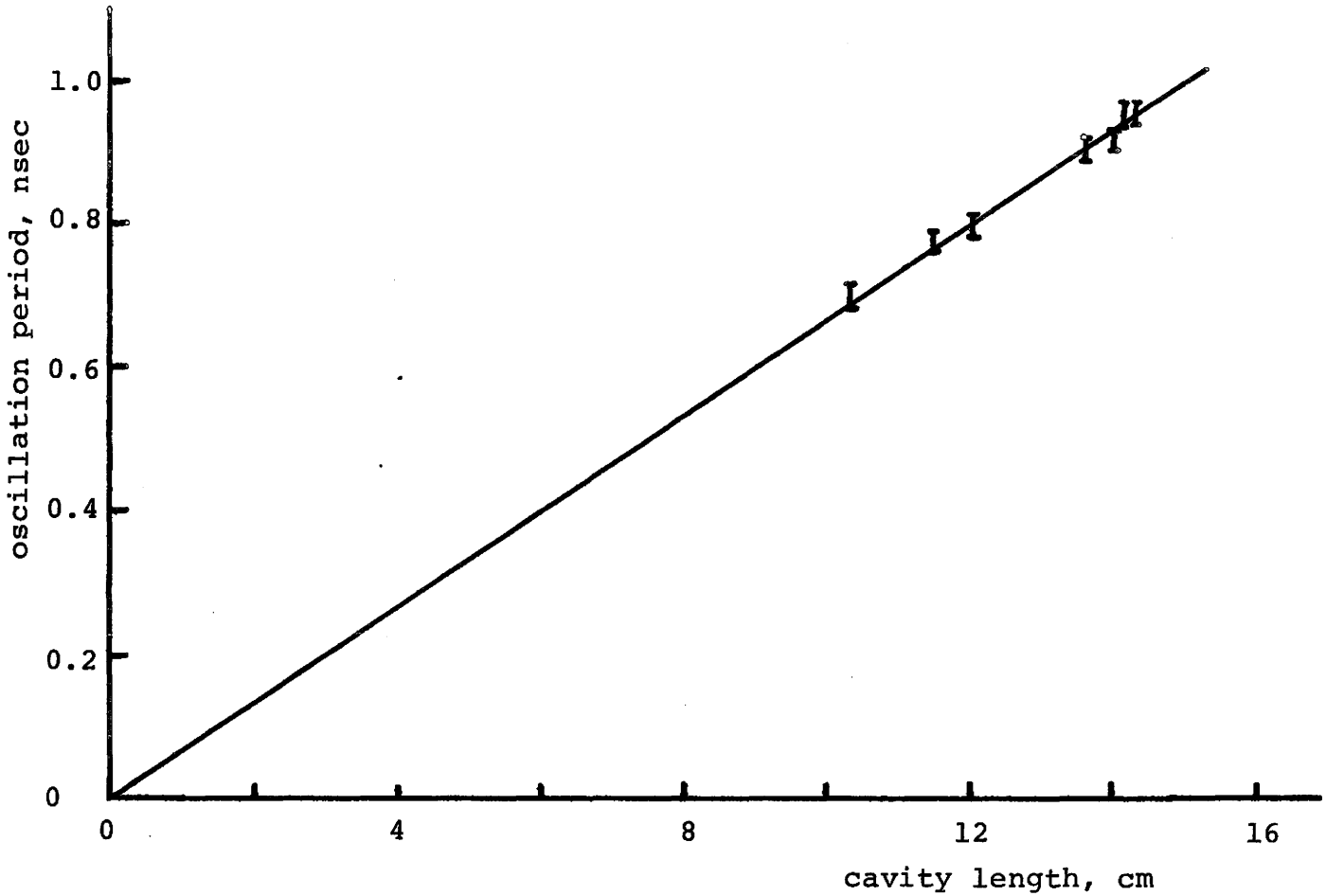

oscillation frequency, the cavity did have a marked effect on the oscillation amplitude and period.

6 OPTOELECTRONIC FEEDBACK

6.1 Experimental Results

Another possibility for feedback with a laser diode is an electrical feedback system where a replica of the optical pulse is electrically injected into the laser. This scheme was described by Damen and Duguay[15]. Their system (figure 6-1) used an optical detector, an amplifier, a diode laser, and an optical feedback path. They started the pulser by increasing the d.c. bias to the laser diode to slightly above threshold, when the circuit would start pulsing. They observed that the optical pulse out was shorter than the regenerated current pulse, and thus the system tended to the shortest current pulse that the amplifier could produce. (Note that here the repetition rate is on a time scale long compared with the laser diode responses, and thus the laser sees each current pulse separately).

The modification made by this author was to add the step recovery diode pulse shaping circuit (figure 2-19). Shaping of the amplified current pulse before it was fed to the laser relaxed amplifier requirements considerably while still enabling generation of optical pulses under 90 psec.

Without the SRD shaper, the current pulses produced by the feedback loop were approximately 2.5 nsec FWHM, and at least three laser relaxation oscillations were produced per current pulse. With the SRD shaper used, the current pulse obtained at maximum gain (57 dB) and d.c. current of 170 mA had a risetime of approximately 100 psec and FWHM of

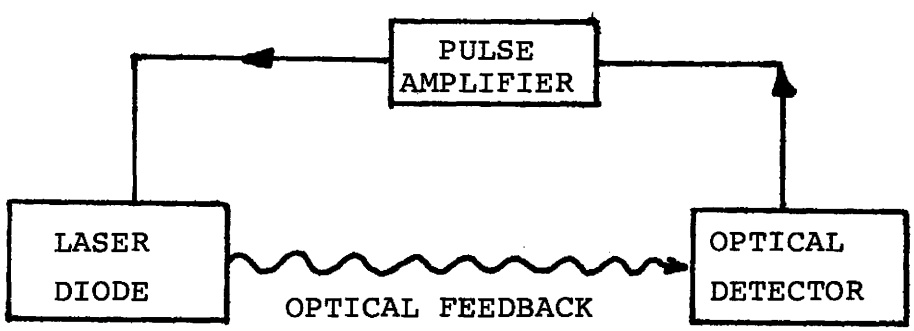

FIGURE 6-1 OPTOELECTRONIC PULSER, REF. 15

500 psec, with a peak amplitude of 200 mA. These currents correspond to $I_{d.c.} = 0.8\ I_{th}$ and $I_{pulse} = I_{th}$. Operation with these circuit parameters produced the optical pulses shown in figures 6-2 a and b. These (signal-averaged) pulses had a FWHM of 110 psec and hence a light pulse width of 80-90 psec, which is much less than the length of the current pulse. Operation of the loop was very stable and the operating point could be adjusted by varying the d.c. laser bias and the two SRD currents.

The high pass filter in the pulse-shaper limited low frequency response to 7 MHz and was necessary to prevent envelope modulation on a micro-second time scale. The current monitor was used as a trigger signal for the sampling oscilloscope; the fast current risetime together with a take-off inside the feedback loop produced a basically jitter-free trigger.

Measurements were conducted to relate the minimum d.c. laser bias for regeneration to the available amplifier gain. It was not possible to determine how much electrical loss occurred in the laser diode mount, and thus absolute gain cannot be stated. However, as figure 6-3 shows, the minimum d.c. operating current was found to be roughly proportional to the logarithm of the amplifier voltage gain.

6.2 Discussion

The simplest way to produce picosecond pulses from diode lasers is to use gain switching. A fast risetime, large amplitude current pulse is applied to the laser diode, causing a rapid population

FIGURE 6-2 REGENERATIVE LASER PULSER OUTPUT

(The pulses in (a) were broadened by the sampling oscilloscope response on this time scale.)

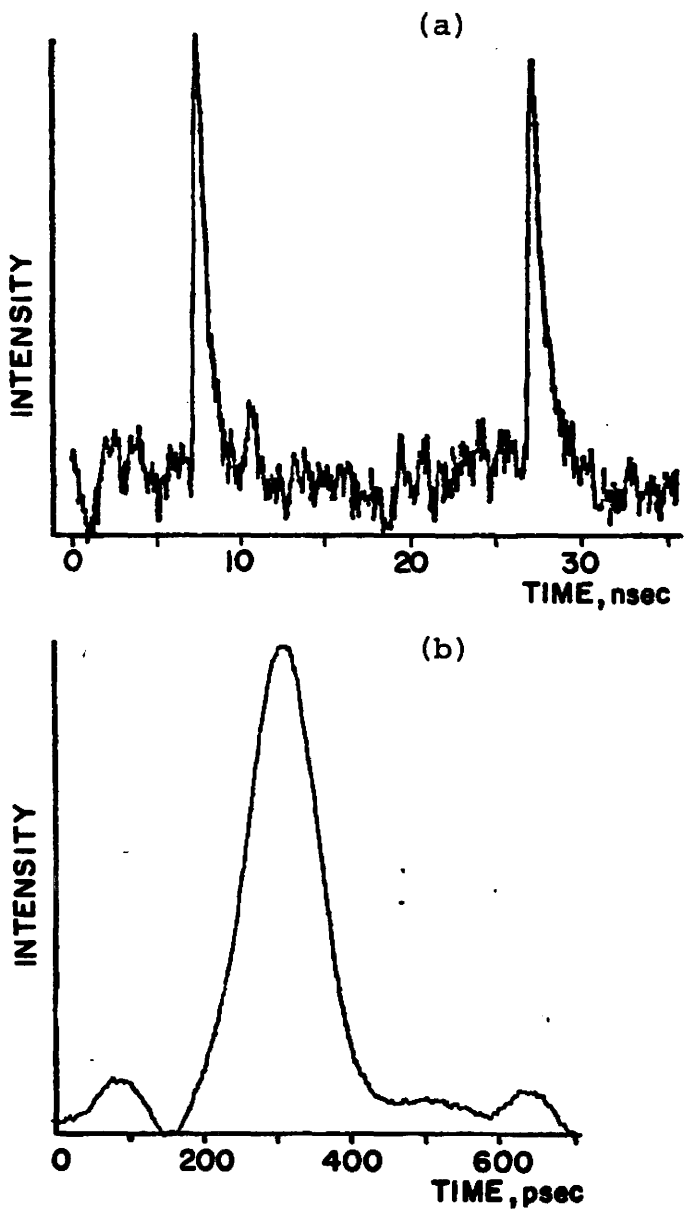

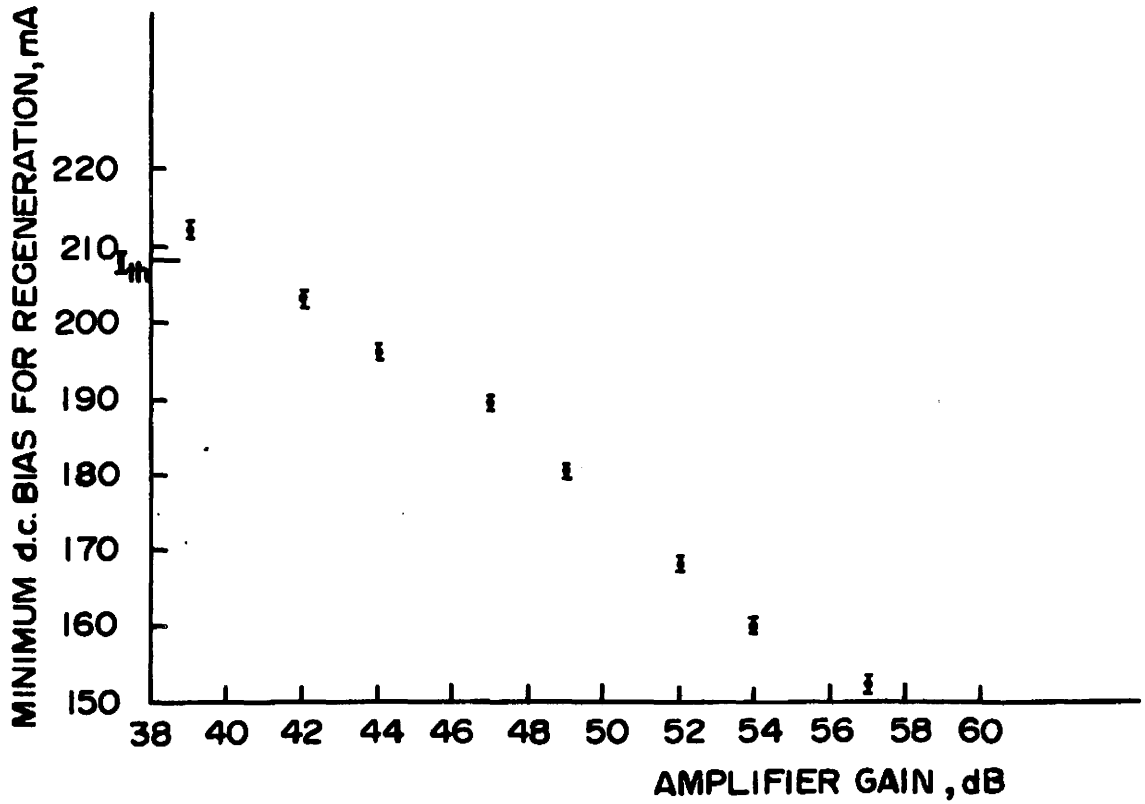

FIGURE 6-3 d.c. REGENERATION BIAS vs. AMPLIFIER GAIN

inversion which overshoots the steady state value, initiating relaxation oscillations. If the current pulse turns off just after the inversion reaches its peak, the lasing action will rapidly deplete the inversion and a single short (20-40 psec) pulse will be emitted.

The optoelectronic regeneration scheme works on this gain switching principle with the current pulse generated using a photodetector, amplifier, and, in this case, pulse shaping circuit. The time delay for the population to cross threshold can be derived from the rate of change of the injected carrier density and is given by equation 3-5

$$t_d \simeq \tau \, \ell n\left[\frac{I_{pk} - I_{dc}}{I_{pk} - I_{th}}\right] \qquad 3\text{-}5$$

The first consequence of this delay is that for low I_{dc}, much of the pumping current is used reaching the inversion threshold, and little is left after the gain crosses threshold. Thus a low amplitude, narrow light pulse will result and the integrated (by the amplifier) optical signal will decrease rapidly with decreasing I_{dc}, requiring much higher loop gain for low I_{dc} as was found experimentally (Fig. 6-3). The second consequence of the delay is that the optoelectronic feedback system operating with I_{dc} less than I_{th} will always tend to the shortest current pulse which the detector-amplifier combination can produce. However, as demonstrated in this work, it is possible to produce current pulses which give results equivalent to those obtained with a fast amplifier by using an SRD pulse shaper and a slow amplifier. The amplifier high frequency response in this case does not have to be much

better than the maximum pulse repetition rate if multiple SRD's are used to shape the pulse. Consequently for a fixed frequency setup at, for example, 100 MHz repetition rate, a one octave, 100-200 MHz detector-amplifier combination with SRDs should be sufficient to produce gain switch limited pulses of approximately 20 psec, since SRD shaping circuits can be designed to give pulses as short as 50 psec[10].

7 CONCLUSIONS

Experiments have been done to characterize the dynamic behaviour of laser diodes. The threshold current and spontaneous carrier lifetime have been measured, and quantitative comparison with computer simulations of relaxation oscillations have shown good agreement for low to moderate pumping. For higher current pumping levels, the mode competition processes are not fully understood, and thus simulations are difficult. Using a single mode laser for the experiments should enable better agreement to be obtained between theory and experiment.

The effects of optical and optelectronic feedback systems were also investigated. The optical feedback, produced using a microscope objective and an external mirror, lowered the d.c. threshold by about 8%. It had a strong effect on the amplitude and frequency of the laser diode relaxation oscillations for external cavity periods on the order of the relaxation oscillation frequencies. For these conditions, the relaxation oscillations were enhanced in amplitude and duration, and occured at the cavity round trip time. Greater optical feedback could be produced with laser diodes which are more optically accessible.

The optoelectronic feedback was used to produce stable, 90 psec light pulses at 50 MHz repetition rates using a simple feedback loop. Small modifications such as an improved pulse shaping circuit and shorter electrical connections should enable generation of 40 psec pulses at over 100 MHz repetition rates.

REFERENCES

1. R.N. Hall, G.E. Fenner, J.D. Kinglsey, T.J. Soltys, R.O. Carlson, "Coherent Light Emission from GaAs Junctions", Phys. Rev. Lett. 9, 366 (1962).

2. M.I. Nathan, W.P. Dumke, G. Burns, F.H. Dill, Jr., G. Lasher, "Stimulated Emission of Radiation from GaAs p-n Junctions", Appl. Phys. Lett. 1, 62 (1962).

3. T.M. Quist, R.H. Rediker, R.J. Keyes, W.E. Krag, B. Lax, A.L. McWhorter, H.J. Ziegler, "Semiconductor Maser of GaAs", Appl. Phys. Lett. 1, 91 (1962).

4. I. Hayashi, M.B. Panish, P.W. Foy, S. Sumski", Junction Lasers Which Operate Continuously at Room Temperature", Appl. Phys. Lett. 17, 109 (1970).

5. H. Kressel, F.Z. Hawrylo, "Fabry-Perot Structure $Al_x Ga_{1-x}$ As Injection Lasers with Room Temperature Threshold Current Densities of 2530 A/cm^2", Appl. Phys. Lett. 17, 169 (1970).

6. M. Arditi, "Characteristics and Applications of Microstrip for Microwave Wiring", I.R.E. Trans. Mic. Theory and Tech. MTT3, 31 (1955).

7. H.R. Kaupp, "Characteristics of Microstrip Transmission Lines", I.E.E.E. Trans. Elec. Computers EC16, 185 (1967).

8. S. John, P. Arlett, "Simple Method for the Calculation of the Characteristic Impedance of Mmicrostrip", Elec. Lett. 10, 188 (1974).

9. Laser Diode Laboratories, Inc. Spec Sheet for LCW-5, LCW-10 Lasers, New Brunswick, N.J.

10. Hewlett-Packard Application Note 918" Pulse and Waveform Generation with Step Recovery Diodes".

11. H. Kressel and J.K. Butler", Semiconductor Lasers and Heterojunction LEDs", Academic Press, New York, 1977.

12. J.C. Goodwin, Private communication, 1980.

13. J.C. Goodwin, Ph.D. Thesis, to be published.

14. R.P. Salathe, "Diode Lasers Coupled to External Resonators", Appl. Phys. 20, 1 (1979).

15. T.C. Damen, M.A. Dugauay, "Optoelectronic Regenerative Pulser", Elec. Lett. 16, 166 (1980).